Relativistic mean field model based on realistic nuclear forces

S. Hirose,[1,*] M. Serra,[1] P. Ring,[1,2] T. Otsuka,[1,3,4] and Y. Akaishi[4,5]
[1]*Department of Physics, University of Tokyo, Hongo, Bunkyo-ku, Tokyo, 113-0033, Japan*
[2]*Physik department, Technische Universität München, Garching, Germany*
[3]*Center for Nuclear Study, University of Tokyo, Hongo, Bunkyoku, Tokyo 113-0033, Japan*
[4]*RIKEN, Hirosawa, Wako-shi, Saitama 351-0198, Japan*
[5]*Nihon University, Funabashi-shi, Chiba 274-8501, Japan*
(Received 10 August 2006; published 8 February 2007)

In order to predict properties of asymmetric nuclear matter, we construct a relativistic mean field (RMF) model consisting of one-meson exchange (OME) terms and point coupling (PC) terms. In order to determine the density dependent parameters of this model, we use properties of isospin symmetric nuclear matter in combination with the information on nucleon-nucleon scattering data, which are given in the form of the density dependent G-matrix derived from Brueckner calculations based on the Tamagaki potential. We show that the medium- and long-range components of this G-matrix can be described reasonably well by our effective OME interaction. In order to take into account the short-range part of the nucleon-nucleon interaction, which cannot be described well in this manner, a point coupling term is added. Its analytical form is taken from a model based on chiral perturbation theory. It contains only one additional parameter, which does not depend on the density. It is, together with the parameters of the OME potentials adjusted to the equation of state of symmetric nuclear matter. We apply this model for the investigation of asymmetric nuclear matter and find that the results for the symmetry energy as well as for the equation of state of pure neutron matter are in good agreement with either experimental data or with presently adopted theoretical predictions. In order to test the model at higher density, we use its equation of state for an investigation of properties of neutron stars.

DOI: 10.1103/PhysRevC.75.024301 PACS number(s): 21.30.Fe, 21.60.−n, 21.10.Hw, 26.60.+c

I. INTRODUCTION

Quantum chromodynamics (QCD) is the fundamental theory of strong interaction and in principle also the basis of the description of nuclei. However, because of the strong nonperturbative effects of QCD at low energies, it is, so far, practically impossible to apply it directly for the study of nuclear properties. On the other hand, in the theory of nuclear structure one has developed with great success several more or less phenomenological theories. Density functional theories (DFT), based on the concept of mean field theory, provide a nearly quantitative description of many nuclear properties all over the periodic table, in particular for medium-heavy and heavy nuclei. Because of the large spin-orbit term characterizing the nuclear fields, it has become very useful to take the Lorentz invariance seriously and to start from covariant density functionals. Such approaches run under the name relativistic mean field (RMF) models.

In such models introduced originally by Walecka [1,2], the nucleons are considered as elementary degrees of freedom. They are expressed in terms of Dirac spinors, and are assumed to interact with each other through effective boson fields, which are characterized by the quantum numbers of parity, spin, and isospin. Within the mean field approximation this interaction is equivalent to the exchange of various effective mesons with the corresponding quantum numbers. These mesons are point-like and they are characterized by their masses and by the vertices describing the coupling to the nucleons. Usually these parameters are determined by a fit to reproduce observables in finite nuclei and in nuclear matter. Within the RMF models it is easy to obtain nuclear saturation and they naturally provide an explanation of the rather strong spin-orbit force [3].

There are two interpretations for the meson included in RMF models. One is that we identify the mesons of the models with mesons observed experimentally. The other is that effects originating from many complicated diagrams in a more microscopic theory which cannot be treated explicitly within mean field calculations are renormalized into the parameters of effective mesons. In this paper, we adopt the second interpretation. There are two reasons for this. First, we would like to stay on the level of only one meson exchange (OME) processes in calculations for actual nuclei because there are well-known divergences occurring in loop diagrams. They are difficult to deal with by numerical methods when we study properties of finite nuclei. This corresponds fully to the concept of density functional theory, where all these effects are taken into account in a phenomenological way. Therefore one expects that the parameters deviate from the bare values. Second, not all the mesons which we need for a realistic description of nuclear properties on the tree level occur in nature as resonances. In order to take into account all the spin and isospin information by OME processes, we need to assign one meson to each spin-isospin channel. Therefore, some mesons occurring in these models do not have an explicit experimental counterpart in a resonance state. On the other hand, by considering loop diagrams it is possible to describe all spin-isospin channels even with a smaller number of mesons.

*Present address: Data Mining Research Group, Internet Systems Research Laboratories, NEC Corporation, Shimonumabe, Kawasaki-shi, 211-8666, Japan.

For example, in chiral perturbation theory (ChPT), where only the π meson is taken into account, it is impossible to reproduce the equation of state (EOS) of nuclear matter considering only tree diagrams, but it may become possible by including loop diagrams [4] and by adjusting the necessary cut-off parameters in a phenomenological way. Compared with ChPT, RMF models can produce reasonably well the EOS with tree diagrams with the price that several phenomenological mesons have to be included.

The simplest model of this category is the $\sigma\omega$-model introduced by Serot and Walecka [2]. In infinite nuclear matter it contains only two adjustable parameters, determined by the saturation point, i.e., by two data. In nuclei with neutron or proton excess one needs at least one additional potential in the isovector channel and therefore in addition to σ and ω the ρ meson is included, which carries isospin.

The incompressibility calculated from this model is too large, about twice as large as the empirical value [5]. This indicates that the surface properties are not described properly in this simple model and therefore the model is relatively useless for a quantitative description of finite nuclei. As pointed out first by Boguta and Bodmer [6], for a realistic description of finite nuclei it is important to include a density dependence and this turned out to be crucial for the success of these models in finite nuclei.

There are two ways to introduce effective density dependencies. One way is to include nonlinear couplings between the mesons [6]. In the mean field approximation, these couplings effectively correspond to density dependent contributions. A number of RMF effective interactions of this type have been developed, such as NL1, NL2 [7], NL3 [8], NL-SH [9], TM1, and TM2 [10]. A part of these higher order self-interactions can be motivated by vacuum renormalization [2,11]. However, in practice, their strength parameters are determined in a purely phenomenological way. As an alternative, density-dependent RMF (DDRMF) models have been proposed in Refs. [12,13] and very successful parameter sets DD-ME1 [14] and DD-ME2 [15] have been determined by precision fits to nuclear data. The density dependence of the coupling constants in these models is motivated by that of Dirac-Brueckner calculations [16,17]. The strength of the meson-nucleon-vertices decreases in these DDRMF models with increasing density more rapidly in the isovector channel than in the isoscalar channel. Therefore, at higher density, these models produce weaker repulsion generated by vector mesons and thus the equation of state (EOS) of DDRMF models is softer than in other RMF models. Both models have been extremely successful in the global description of ground-state, single-particle, and collective properties of nuclei all over the periodic table [10,18–20].

Comparing with nonrelativistic density functionals, there are some advantages for using covariant functionals, i.e., RMF models when studying properties of finite nuclei. An important example is the relativistic quenching of the isoscalar attraction in these models, which provides a very simple saturation mechanism. In nonrelativistic models a phenomenological contact term has to be introduced, which is strongly density dependent. Also very important is the fact that the large spin-orbit splitting in finite nuclei is a relativistic effect and therefore it is included in relativistic models in a natural way without any further adjustment of the parameters. Already the simplest $\sigma\omega$-model with only two parameters determined by the saturation properties of nuclear matter produces a spin-orbit term with the right sign and the proper size. These advantages are features which have to be built into nonrelativistic models at the cost of additional phenomenological parameters.

In all density functionals, relativistic or nonrelativistic, the effective interactions are determined to a large extent by observed properties of nuclei in and close to the valley of stability. Therefore, there remains room for discussions as to whether the isospin dependence of these effective interactions is appropriate and also as to whether they can be extrapolated to nuclei with extreme conditions of isospin and/or density.

In such a situation, Serra *et al*. [21] proposed in a fully microscopic investigation to derive the parameters of DDRMF models directly from the nucleon-nucleon (*NN*) interaction. The G-matrix calculated from the bare nucleon-nucleon interaction of Tamagaki *et al* [22] was used to derive the parameters of a RMF model. Independently from the properties of specific finite nuclei, one is able in this way to determine not only the density dependence of the meson-nucleon couplings, but also that of the meson masses in all four meson channels, scalar/vector as well as isoscalar/isovector. On the other hand, the density dependence determined in this fully microscopic way appeared rather similar to that of phenomenological models obtained by fitting to finite nuclei [14,15]. This microscopic model is, however, not sufficiently good to reproduce experimental data in finite nuclei or in nuclear matter. In particular there is no saturation, because the model of Serra *et al*. [21] is not designed to take into account, to a sufficient accuracy, the behavior of the effective nucleon-nucleon (*NN*) forces at short distances.

In this paper, we first construct a DDRMF model along the same line as proposed by Serra *et al*. [21]. Since the short-range behavior of effective forces is determined by physical processes at higher momentum transfer, we use a philosophy similar to the one in the chiral perturbation theory, and introduce phenomenological zero-range forces so as to describe the short-range behavior. In addition we adjust the density dependence of our model parameters not only to the parameter-free G-matrix results obtained from the *NN*-potential, as it was done by Serra *et al*. [21], but also to the density dependence of the EOS in symmetric nuclear matter. In this way we obtain a model, which describes not only the effective nuclear force, but also the density dependence of symmetric nuclear matter including its saturation properties. This model is then examined for two applications. First, we investigate the properties of asymmetric nuclear matter and find excellent agreement with the microscopic calculations of Freedman and Phandaripande [23] up to relatively high densities. Secondly, we use this EOS for the calculation of neutron stars and the corresponding mass limitations.

The paper is organized as follows. In Sec. II we introduce the one meson exchange part of our model and we discuss how the resulting interactions can be compared with the nonrelativistic G-matrix potentials derived from the bare *NN* interaction. In Sec. III we present analytical formulas for the calculation of the corresponding OME energies expanding up

to the fourth order in k_f/M. The point coupling terms are introduced in Sec. IV, and in Sec. V we determine the parameters of the model and discuss their density dependencies. In Sec. VI we apply our model to the asymmetric nuclear matter and compare it with other theories on this subject. As an application of the EOS thus obtained, we consider in Sec. VII neutron stars and discuss their properties. Section VIII contains a summary and an outlook to future applications of this model.

II. THE MESON EXCHANGE POTENTIAL

We first discuss the one-meson exchange part of our model. Its Lagrangian is given by

$$\begin{aligned}\mathcal{L}_{\rm OME} &= \bar\psi(i\gamma^\mu\partial_\mu - M)\psi + \frac{1}{2}\left(\partial^\mu\sigma\,\partial_\mu\sigma - m_\sigma^2\sigma^2\right)\\ &+ \frac{1}{2}\left(\partial^\mu\vec\delta\partial_\mu\vec\delta - m_\delta^2\vec\delta^2\right) + \frac{1}{2}\left(\partial^\mu\vec\pi\,\partial_\mu\vec\pi - m_\pi^2\vec\pi^2\right)\\ &+ \left[-\frac{1}{4}\omega^{\mu\nu}\omega_{\mu\nu} + \frac{1}{2}m_\omega^2\omega^\mu\omega_\mu\right]\\ &+ \left[-\frac{1}{4}\vec\rho^{\mu\nu}\vec\rho_{\mu\nu} + \frac{1}{2}m_\rho^2\vec\rho^\mu\vec\rho_\mu\right] - g_\sigma\bar\psi\psi\sigma - g_\delta\bar\psi\vec\tau\psi\vec\delta\\ &- g_\omega\bar\psi\gamma^\mu\psi\omega_\mu - g_\rho\bar\psi\gamma^\mu\vec\tau\psi\vec\rho_\mu - \frac{f_\pi}{m_\pi}\bar\psi\gamma_5\gamma^\mu\vec\tau\psi\partial_\mu\vec\pi\\ &- \frac{f_\rho}{4M}\bar\psi\frac{i}{2}[\gamma^\mu,\gamma^\nu]\vec\tau\psi\vec\rho_{\mu\nu} \qquad (1)\end{aligned}$$

with

$$\omega_{\mu\nu} \equiv \partial_\mu\omega_\nu - \partial_\nu\omega_\mu, \qquad \vec\rho_{\mu\nu} \equiv \partial_\mu\vec\rho_\nu - \partial_\nu\vec\rho_\mu. \qquad (2)$$

This Lagrangian contains an isoscalar scalar σ-field, an isovector scalar δ-field, an isovector pseudoscalar π-field (pseudovector coupling), and an isoscalar vector ω-field (only vector coupling), and an isovector vector ρ-field (vector and tensor couplings). As compared to many other RMF models we here include a δ-meson field, a π-meson field with the pseudovector coupling, and a tensor coupling term for the ρ-meson.

Since our parameters (masses and coupling constants) are density dependent, we do not take into account additional nonlinear self-coupling terms for the σ or ω meson. We also neglect a tensor coupling of the ω meson although we introduce a pseudovector coupling of the π meson and a tensor coupling of the ρ meson. We adopt this "unbalanced" Lagrangian for two reasons. First, the contribution from the tensor coupling term of the ω meson is negligible when we use the known value for f_ω ($f_\omega/g_\omega = -0.12$). Second, the contributions from these two terms turn out to be negligibly small if we allow the corresponding parameters to be adjusted by a free fit as discussed below.

The parameters of the OME part are determined by comparing with the nonrelativistic G-matrix derived from the bare *NN* interaction of Tamagaki *et al*. [22]. For this purpose we have to perform a nonrelativistic reduction of the RMF terms in Eq. (1). We choose this reduction because non-relativistic G-matrix calculations are well under control and therefore we expect to obtain in this way reliable information on the properties particularly in the isospin $T = 1$ channel, which is difficult to access in phenomenological fits of RMF parameters based primarily on data of nuclei on or close to the stability line.

We treat the masses and coupling constants of the mesons as adjustable parameters. These parameters are determined by comparing the radial shape of the G-matrix potentials, as explained below, with that of the OME potentials derived from the RMF Lagrangian after a nonrelativistic reduction. Since the results of the G-matrix calculations include medium effects and depend therefore on the density, we find in this way density dependent masses and couplings naturally.

Starting from the bare *NN* interaction of Tamagaki and Takatsuka [22] which was fitted to reproduce *NN* scattering data up to 350 [MeV] and by adopting Brueckner's G-matrix formalism [24], we derived a realistic effective interaction in nuclear matter. The introduction of the G-matrix is necessitated by the singular nature of the two-body forces at short distances, namely, the repulsive core and the existence of a strong noncentral part. Usually the G-matrix is given in terms of matrix elements in a certain configuration space. The method of Nagata, Bando, and Akaishi [25] allows us to represent the G-matrix not only in terms of matrix elements but in a local approximation also in the form of an effective two-body potential depending on the relative coordinate $\mathbf{r} = \mathbf{r}_1 - \mathbf{r}_2$ as well as spin and isospin variables. The actual potentials are represented as appropriate superpositions of various Gaussian functions centered at the origin. These potentials depend on the nuclear density. At the densities relevant for this investigation this local approximation of the G-matrix is in good agreement with the full G-matrix

Since we are interested, at this point, in the inclusion of the basic features of realistic interactions at medium and long distances, it is not necessary to represent the G-matrix very precisely at short distances. Therefore, the potential representation scheme in Ref. [25] plays a very essential role. The bare potential is taken from Ref. [22], though other realistic potentials could have been used too.

In Figs. 1 and 2, we show the G-matrix potentials (Akaishi potential [21]) in the ^{1}O, ^{3}O, ^{1}E, and ^{3}E channels as a function of the internucleon distance. We see that the ^{3}E potential becomes strongly attractive due to the renormalization of the bare tensor force. Without it, the ^{3}E potential is less attractive than the ^{1}E potential by a factor of two. The ^{3}E potential also has a stronger density dependence than the ^{1}E potential, and this difference has its origin almost completely in the renormalization of the bare tensor force. Clearly these two potentials, ^{1}E and ^{3}E, give the main contribution to the nuclear binding, because the other terms like the LS interaction are rather weak on the whole.

Using the projections operators $\Pi_{s(t)}^{\sigma(\tau)}$ onto the singlet (s) and triplet (t) parts of the nucleon two-body wave functions in spin (σ) and isospin (τ) space we decompose the central potential $\mathcal{V}_c$ to the form

$$\begin{aligned}\mathcal{V}_c(r) &= \mathcal{V}_{\rm te}(r)\Pi_t^\sigma\,\Pi_s^\tau + \mathcal{V}_{\rm se}(r)\Pi_s^\sigma\,\Pi_t^\tau\\ &+ \mathcal{V}_{\rm to}(r)\Pi(r)_t^\sigma\,\Pi_t^\tau + \mathcal{V}_{\rm so}(r)\Pi_s^\sigma\,\Pi_s^\tau. \qquad (3)\end{aligned}$$

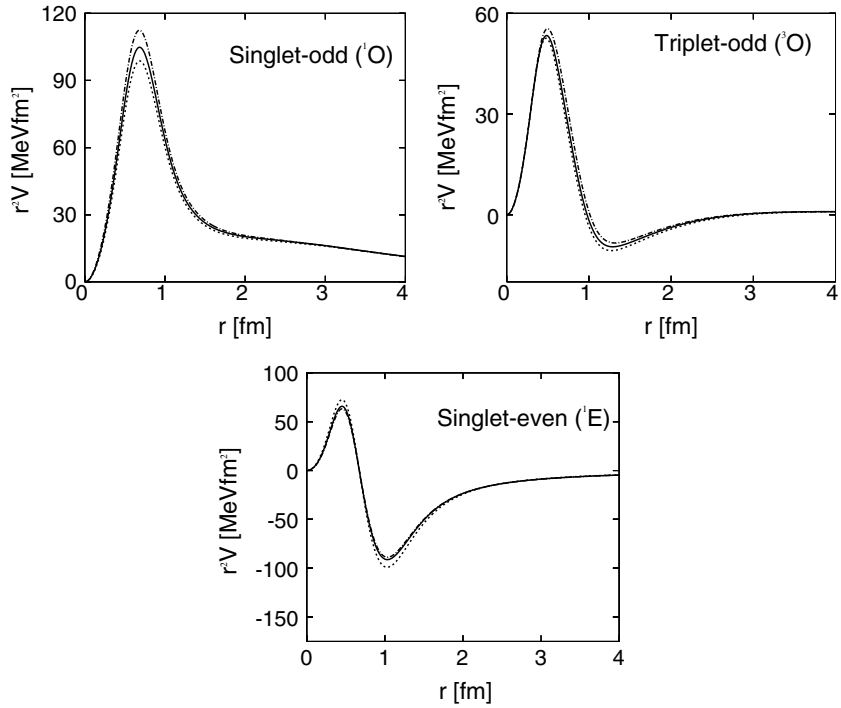

FIG. 1. G-matrix potentials in the ^{1}O, ^{3}O, and ^{1}E channels. Dashed, solid, and dashed-dotted lines represent the potentials at the density, $k_f = 1.0$ fm^{-1}, $k_f = 1.4$ fm^{-1}, and $k_f = 1.8$ fm^{-1}, respectively.

Replacing the projection operators by spin and isospin operators, $\mathcal{V}_c$ can be rewritten as follows:

$$\mathcal{V}_c(r) = \mathcal{V}_0(r) + \mathcal{V}_\sigma(r)\boldsymbol{\sigma}\cdot\boldsymbol{\sigma} + \mathcal{V}_\tau(r)\boldsymbol{\tau}\cdot\boldsymbol{\tau} + \mathcal{V}_{\sigma\tau}(r)(\boldsymbol{\sigma}\cdot\boldsymbol{\sigma})(\boldsymbol{\tau}\cdot\boldsymbol{\tau}). \tag{4}$$

The potentials, $\mathcal{V}_0$, $\mathcal{V}_\sigma$, $\mathcal{V}_\tau$, and $\mathcal{V}_{\sigma\tau}$ can be expressed in terms of the potentials $\mathcal{V}_{\rm te}$, $\mathcal{V}_{\rm se}$, $\mathcal{V}_{\rm to}$, and $\mathcal{V}_{\rm so}$ as

$$\begin{aligned}
\mathcal{V}_0 &= \tfrac{1}{16}(3\mathcal{V}_{\rm te} + 3\mathcal{V}_{\rm se} + 9\mathcal{V}_{\rm to} + \mathcal{V}_{\rm so}),\\
\mathcal{V}_\sigma &= \tfrac{1}{16}(\mathcal{V}_{\rm te} - 3\mathcal{V}_{\rm se} + 3\mathcal{V}_{\rm to} - \mathcal{V}_{\rm so}),\\
\mathcal{V}_\tau &= \tfrac{1}{16}(-3\mathcal{V}_{\rm te} + \mathcal{V}_{\rm se} + 3\mathcal{V}_{\rm to} - \mathcal{V}_{\rm so}),\\
\mathcal{V}_{\sigma\tau} &= \tfrac{1}{16}(-\mathcal{V}_{\rm te} - \mathcal{V}_{\rm se} + \mathcal{V}_{\rm to} + \mathcal{V}_{\rm so}).
\end{aligned} \tag{5}$$

In Fig. 3, the local potentials $\mathcal{V}_0, \mathcal{V}_\sigma, \mathcal{V}_\tau, \mathcal{V}_{\sigma\tau}$, the two-body LS potential $\mathcal{V}_{\rm LS}$, and the tensor potential $\mathcal{V}_T$ are plotted as a function of the relative distance r for three values of the density.

In order to compare an RMF model with the realistic effective interaction in the medium, we start with the relativistic OME amplitudes in momentum space [26]. The Lagrangian in Eq. (1) leads to the following OME amplitudes:

$$\begin{aligned}
\langle \mathbf{q}'\lambda_1'\lambda_2'|V^{\rm OME}_{\sigma,\delta}|\mathbf{q}\lambda_1\lambda_2\rangle &= -\frac{g_\phi^2}{(\mathbf{q}'-\mathbf{q})^2+m_\phi^2}\bar{u}(\mathbf{q}',\lambda_1')u(\mathbf{q},\lambda_1)\\
&\quad\times\bar{u}(-\mathbf{q}',\lambda_2')u(-\mathbf{q},\lambda_2),\\
\langle \mathbf{q}'\lambda_1'\lambda_2'|V^{\rm OME}_{\pi}|\mathbf{q}\lambda_1\lambda_2\rangle &= -\frac{(f_\pi/m_\pi)^2}{(\mathbf{q}'-\mathbf{q})^2+m_\phi^2}\bar{u}(\mathbf{q}',\lambda_1')\gamma_5\gamma^\mu\\
&\quad\times(q'-q)_\mu u(\mathbf{q},\lambda_1)\bar{u}(-\mathbf{q}',\lambda_2')\gamma_5\gamma^\nu(q'-q)_\nu u(-\mathbf{q},\lambda_2),\\
\langle \mathbf{q}'\lambda_1'\lambda_2'|V^{\rm OME}_{\omega,\rho}|\mathbf{q}\lambda_1\lambda_2\rangle &= \frac{1}{(\mathbf{q}'-\mathbf{q})^2+m_\phi^2}\\
&\quad\times\left[g_\phi\bar{u}(\mathbf{q}',\lambda_1')\gamma_\mu u(\mathbf{q},\lambda_1) - \frac{f_\phi}{2M}\bar{u}\right.\\
&\quad\left.\times(\mathbf{q}',\lambda_1')\frac{1}{2}[\gamma_\mu,\gamma_\nu](q'-q)^\nu u(\mathbf{q},\lambda_1)\right]\\
&\quad\times\left[g_\phi\bar{u}(-\mathbf{q}',\lambda_2')\gamma_\mu u(-\mathbf{q},\lambda_2) + \frac{f_\phi}{2M}\bar{u}(-\mathbf{q}',\lambda_2')\right.\\
&\quad\left.\times\frac{1}{2}[\gamma_\mu,\gamma_\nu](q'-q)^\nu u(-\mathbf{q},\lambda_2)\right],
\end{aligned} \tag{6}$$

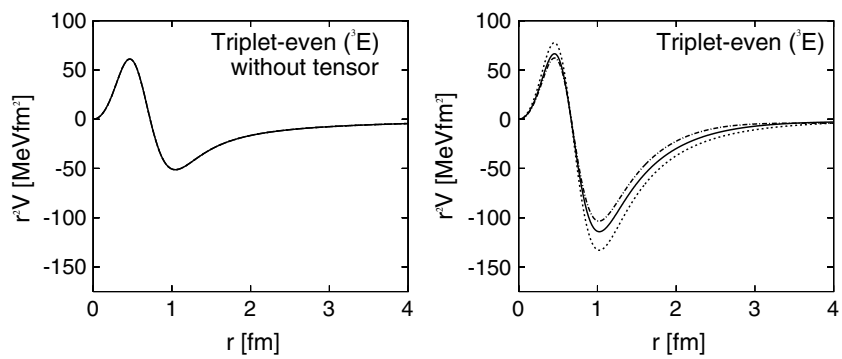

FIG. 2. G-matrix potential in the ^{3}E channel. In the left (right) figure, the tensor interaction is excluded (included). Dashed, solid, and dashed-dotted lines represent the potentials at the density, $k_f = 1.0$ fm^{-1}, $k_f = 1.4$ fm^{-1}, and $k_f = 1.8$ fm^{-1}, respectively. In the left figure they are on top of each other.

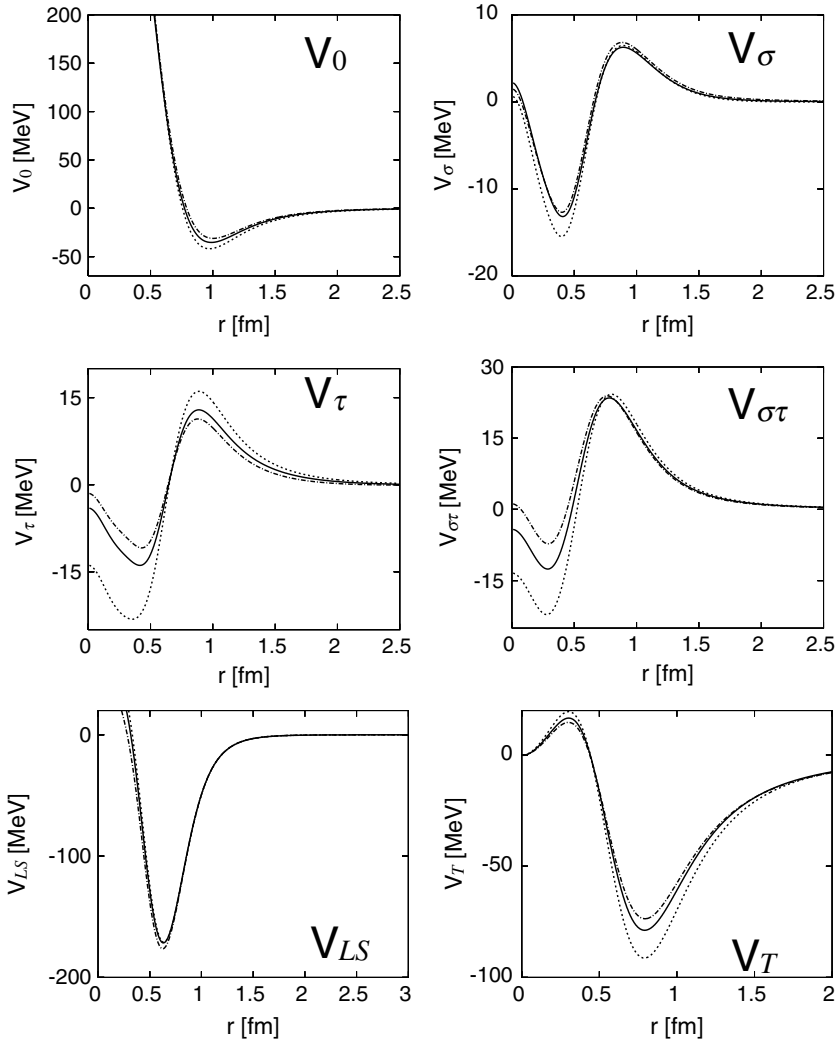

FIG. 3. G-matrix potentials as a function of the relative distance r. Dashed, solid, and dashed-dotted lines represent the potentials at the density, $k_f = 1.0$ fm^{-1}, $k_f = 1.4$ fm^{-1}, and $k_f = 1.8$ fm^{-1}, respectively.

where λ denotes the helicity. From here on, ϕ represents the various mesons ($\phi = \sigma, \delta, \pi, \omega, \rho$) and for simplicity, we do not write isospin operator $\boldsymbol{\tau}_1 \cdot \boldsymbol{\tau}_2$ explicitly. In order to simplify the expressions we use Dirac spinors in the representation

$$u(\mathbf{q}, s) = \left(\frac{E+M}{2M}\right)^{1/2} \begin{pmatrix} 1 \\ \frac{\sigma \cdot \mathbf{q}}{E+M} \end{pmatrix} \chi_s, \tag{7}$$

with the Pauli spinor χ_s. We define two momentum variables $\mathbf{p}$ and $\mathbf{k}$ as

$$\mathbf{p} = \tfrac{1}{2}(\mathbf{q}' + \mathbf{q}), \quad \mathbf{k} = \mathbf{q}' - \mathbf{q}. \tag{8}$$

Using Eq. (7) and expanding in a standard nonrelativistic reduction in powers of p/M and k/M, we obtain the following *reduced* expression in momentum space:

$$V_{\sigma,\delta} = -\frac{g_\phi^2}{\mathbf{k}^2 + m_\phi^2}\left[1 - \frac{\mathbf{p}^2}{2M^2} + \frac{\mathbf{k}^2}{8M^2} - \frac{i}{2M^2}\mathbf{S}\cdot(\mathbf{k}\times\mathbf{p})\right],$$

$$V_\pi = -\frac{f_\pi^2}{m_\pi^2}\frac{(\boldsymbol{\sigma}_1 \cdot \mathbf{k})(\boldsymbol{\sigma}_2 \cdot \mathbf{k})}{\mathbf{k}^2 + m_\pi^2},$$

$$\begin{aligned} V_{\omega,\rho} = \frac{1}{\mathbf{k}^2 + m_\phi^2}\Bigg[& g_\phi^2\Bigg[1 + \frac{3\mathbf{p}^2}{2M^2} - \frac{\mathbf{k}^2}{8M^2} + \frac{3i}{2M^2}\mathbf{S}\cdot(\mathbf{k}\times\mathbf{p}) \\ & - \boldsymbol{\sigma}_1 \cdot \boldsymbol{\sigma}_2 \frac{\mathbf{k}^2}{4M^2} + \frac{1}{4M^2}(\boldsymbol{\sigma}_1 \cdot \mathbf{k})(\boldsymbol{\sigma}_2 \cdot \mathbf{k})\Bigg] \\ & + \frac{g_\phi f_\phi}{2M}\Bigg[-\frac{\mathbf{k}^2}{M} + \frac{i}{4M}\mathbf{S}\cdot(\mathbf{k}\times\mathbf{p}) - \boldsymbol{\sigma}_1 \cdot \boldsymbol{\sigma}_2 \frac{\mathbf{k}^2}{M} \\ & + \frac{1}{M}(\boldsymbol{\sigma}_1 \cdot \mathbf{k})(\boldsymbol{\sigma}_2 \cdot \mathbf{k})\Bigg] \\ & + \frac{f_\phi^2}{4M^2}\Big[-\boldsymbol{\sigma}_1 \cdot \boldsymbol{\sigma}_2 \mathbf{k}^2 + (\boldsymbol{\sigma}_1 \cdot \mathbf{k})(\boldsymbol{\sigma}_2 \cdot \mathbf{k})\Big]\Bigg], \end{aligned} \tag{9}$$

where $\mathbf{S} = \frac{1}{2}(\boldsymbol{\sigma}_1 + \boldsymbol{\sigma}_2)$ is the total spin of the two-nucleon system. In Eq. (9), nonlocalities arise due to the $\mathbf{p}$ and $\mathbf{k}\times\mathbf{p}$ terms. The $\mathbf{p}$ terms provide $Y\nabla + \nabla Y$ terms in coordinate space (Y is a Yukawa function) and the $\mathbf{k}\times\mathbf{p}$ terms lead to the orbital angular momentum operator. Neglecting $\mathbf{p}$ terms, which give only small contributions to the EOS, and contact interaction terms in coordinate space, a standard Fourier transformation is performed. We then obtain the nonrelativistic

OME potentials in coordinate space,

$$\begin{aligned}
\mathcal{V}_0 &= \frac{m_\omega}{4\pi} {g_\omega}^2 \left[1 + \frac{1}{2}\left(\frac{m_\omega}{M}\right)^2\right] Y(m_\omega r) \\
&\quad - \frac{m_\sigma}{4\pi} {g_\sigma}^2 \left[1 - \frac{1}{4}\left(\frac{m_\sigma}{M}\right)^2\right] Y(m_\sigma r), \\
\mathcal{V}_\sigma &= \frac{m_\omega}{24\pi} {g_\omega}^2 \left(\frac{m_\omega}{M}\right)^2 Y(m_\omega r), \\
\mathcal{V}_\tau &= \frac{m_\rho}{4\pi} {g_\rho}^2 \left[1 + \frac{1}{2}\left(1 + \frac{f_\rho}{g_\rho}\right)\left(\frac{m_\rho}{M}\right)^2\right] Y(m_\rho r) \\
&\quad - \frac{m_\delta}{4\pi} {g_\delta}^2 \left[1 - \frac{1}{4}\left(\frac{m_\delta}{M}\right)^2\right] Y(m_\delta r), \\
\mathcal{V}_{\sigma\tau} &= \frac{m_\rho}{24\pi} {g_\rho}^2 \left(1 + \frac{f_\rho}{g_\rho}\right)^2 \left(\frac{m_\rho}{M}\right)^2 Y(m_\rho r) \\
&\quad + \frac{m_\pi}{3}\left(\frac{{f_\pi}^2}{4\pi}\right) Y(m_\pi r), \\
\mathcal{V}_{\mathrm{LS}} &= -\frac{m_\sigma}{8\pi} {g_\sigma}^2 Z_1(m_\sigma r) - \frac{3m_\omega}{8\pi} {g_\omega}^2 Z_1(m_\omega r) \\
&\quad - \frac{m_\delta}{8\pi} {g_\delta}^2 Z_1(m_\delta r) - \frac{3m_\rho}{8\pi} {g_\rho}^2 \left(1 + \frac{4f_\rho}{3g_\rho}\right) Z_1(m_\rho r), \\
\mathcal{V}_T &= -\frac{m_\omega}{48\pi} {g_\omega}^2 Z(m_\omega r) - \left(\frac{{f_\pi}^2}{4\pi}\right) m_\pi Z(m_\pi r) \\
&\quad + \frac{3m_\rho}{48\pi} {g_\rho}^2 \left(1 + \frac{f_\rho}{g_\rho}\right)^2 Z(m_\rho r).
\end{aligned} \tag{10}$$

Here, we define Y, Z, and Z_1 as

$$\begin{aligned}
Y(mr) &\equiv \exp[-mr]/mr, \\
Z(mr) &\equiv \left(\frac{m}{M}\right)^2 \left(1 + \frac{3}{mr} + \frac{3}{m^2 r^2}\right) Y(mr), \\
Z_1(mr) &\equiv \left(\frac{m}{M}\right)^2 \left(\frac{1}{mr} + \frac{1}{m^2 r^2}\right) Y(mr).
\end{aligned} \tag{11}$$

In Eq. (10), $\mathcal{V}_0$, $\mathcal{V}_\sigma$, $\mathcal{V}_\tau$, and $\mathcal{V}_{\sigma\tau}$ are local potentials and are defined as the radial part of each channel of the central potential $\mathcal{V}_c$ [see Eq. (4)]. On the other hand, $\mathcal{V}_{\mathrm{LS}}$ and $\mathcal{V}_T$ are nonlocal potentials. The potentials $\mathcal{V}_{\mathrm{LS}}$ and $\mathcal{V}_T$ in Eq. (10) are written in the form projected onto the ^{3}E channel.

III. ENERGIES IN NUCLEAR MATTER

In this section we present a method for calculating the energy per particle. For a Fermi gas of symmetric nuclear matter the density ρ and the Fermi momentum k_f are related by

$$\rho = \frac{2}{3\pi^2} k_f^3. \tag{12}$$

For asymmetric nuclear matter, where the densities ρ_p and ρ_n for protons and neutrons and the corresponding Fermi momenta k_p and k_n are different, the asymmetry parameter is usually used

$$\alpha = \frac{\rho_n - \rho_p}{\rho_n + \rho_p} \tag{13}$$

with the relations

$$k_p = k_f(1-\alpha)^{1/3} \quad \text{and} \quad k_n = k_f(1+\alpha)^{1/3}. \tag{14}$$

Following the notation that ϕ stands for one of the various mesons ($\phi = \sigma, \delta, \pi, \omega, \rho$), we introduce the following abbreviations:

$$u_{p\phi} \equiv \frac{k_p}{m_\phi}, \quad u_{n\phi} \equiv \frac{k_n}{m_\phi}, \quad u_\phi \equiv \frac{k_f}{m_\phi}. \tag{15}$$

In the calculations of nuclear matter with a finite density, the propagator for a nucleon with the four-momentum $p^\mu = (p^0, \mathbf{p})$ and the mass M in the nuclear medium takes the form

$$\begin{aligned}
&\frac{i}{(2\pi)^4}(\not{p} + M)\left[\frac{1}{p^2 - M^2 + i\epsilon}\right. \\
&\left. + 2i\pi\delta(p^2 - M^2)\theta(p_0)\theta(k_f - |\mathbf{p}|)\right].
\end{aligned} \tag{16}$$

It is comprised of the vacuum part and a medium insertion. Diagrams including no medium insertion lead to an unobservable shift of the vacuum energy. Diagrams including only one medium insertion just renormalizes the nucleon mass to the observed value M, because they include one single on-shell delta function. Therefore, we only calculate diagrams with two medium insertions.

Equation (16) is applied to isospin-symmetric nuclear matter. When dealing with isospin-asymmetric nuclear matter, we have to replace the second part as

$$\theta(k_f - |\mathbf{p}|) \to \frac{1+\tau_3}{2}\theta(k_p - |\mathbf{p}|) + \frac{1-\tau_3}{2}\theta(k_n - |\mathbf{p}|). \tag{17}$$

One of the contributions to the energy per particle

$$\bar{E} = \frac{E}{A} \tag{18}$$

is the kinetic energy of a noninteracting relativistic Fermi gas of nucleons

$$\bar{E}_{\mathrm{kin}}(k_p, k_n) = \frac{2}{\rho} \sum_{\tau=p,n} \int_{p<k_\tau} \frac{d^3p}{(2\pi)^3} \left(\sqrt{\mathbf{p}^2 + M^2} - M\right), \tag{19}$$

where the index τ in the sum runs over protons and neutrons. We apply a nonrelativistic approximation and expand $\sqrt{M^2 + \mathbf{p}^2} - M$ in powers of p/M. Integrating over the Fermi spheres of protons and neutrons, one obtains

$$\begin{aligned}
\bar{E}_{\mathrm{kin}}(k_p, k_n) &= \frac{M}{u_{pM}^3 + u_{nM}^3}\left[\frac{3}{10}\left(u_{pM}^5 + u_{nM}^5\right)\right. \\
&\left. - \frac{3}{56}\left(u_{pM}^7 + u_{nM}^7\right)\right].
\end{aligned} \tag{20}$$

Here, like Eq. (15) in the case of mesons, we introduce the abbreviations

$$u_{pM} \equiv \frac{k_p}{M}, \quad u_{nM} \equiv \frac{k_n}{M}, \quad u_M \equiv \frac{k_f}{M}. \tag{21}$$

Using the two diagrams in Fig. 4, we calculate the OME energy per particle in nuclear matter. These are diagrams with

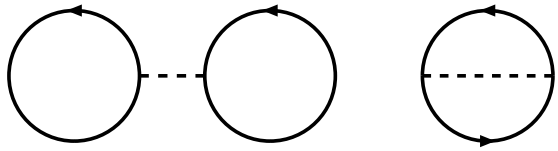

FIG. 4. One meson exchange Hartree diagram (left) and Fock diagram (right). Solid and dashed lines represent a nucleon and each meson (σ, δ, π, ω, ρ), respectively.

two medium insertions. Thus, two-loop integration becomes the integration in Fermi sphere, and no divergence appears. Performing an $1/M$-expansion of the complete integrand, it becomes possible to integrate analytically. We then obtain the OME contributions to the energy per particle

$$\bar{E}_{\rm OME}(k_p, k_n) = \sum_{\phi=\sigma,\delta,\omega,\rho,\pi} \bar{E}_\phi(k_p, k_n) \tag{22}$$

with

$$\bar{E}_\phi(k_p, k_n) = \sum_{\tau\tau'} C_H^\phi(\tau\tau') E_H^\phi(u_{\tau\phi}, u_{\tau'\phi}) + C_F^\phi(\tau\tau') E_F^\phi(u_{\tau\phi}, u_{\tau'\phi}). \tag{23}$$

The coefficients, $C_{H,F}^\phi(pp) = C_{H,F}^\phi(nn)$ and $C_{H,F}^\phi(pn)$ are statistical factors describing the isospin dependence with actual values being given in Table I. The indices H and F denote the contribution from Hartree and Fock diagrams from each meson, respectively.

The energies E_H^ϕ and E_H^ϕ are shown explicitly in Eq. (24). E_H^π vanishes, because the momentum which π meson carries is zero,

$$E_H^{\sigma,\delta}(u_{p\phi}, u_{n\phi}) = -\frac{3g_\phi^2 m_\phi}{64\pi^2 u_\phi^3}\left[f_1(u_{p\phi}, u_{n\phi}) - \left(\frac{m_\phi}{M}\right)^2 \times f_2(u_{p\phi}, u_{n\phi}) + \left(\frac{m_\phi}{M}\right)^4 f_5(u_{p\phi}, u_{n\phi})\right],$$

$$E_H^{\omega,\rho}(u_{p\phi}, u_{n\phi}) = \frac{3g_\phi^2 m_\phi}{64\pi^2 u_\phi^3} f_1(u_{p\phi}, u_{n\phi}),$$

$$E_F^{\sigma,\delta}(u_{p\phi}, u_{n\phi}) = \frac{3g_\phi^2 m_\phi}{128\pi^2 u_\phi^3}\left[f_3(u_{p\phi}, u_{n\phi}) + \frac{1}{4}\left(\frac{m_\phi}{M}\right)^2 [f_1(u_{p\phi}, u_{n\phi}) - f_3(u_{p\phi}, u_{n\phi}) - 2f_4(u_{p\phi}, u_{n\phi})] - \frac{1}{8}\left(\frac{m_\phi}{M}\right)^4 [2f_2(u_{p\phi}, u_{n\phi}) - f_4(u_{p\phi}, u_{n\phi})]\right],$$

TABLE I. Isospin dependent factors $C_H^\phi(\tau\tau')$ for the Hartree contribution and $C_F^\phi(\tau\tau')$ for the Fock one.

	$C_H^\phi(pp)$	$C_H^\phi(pn)$	$C_F^\phi(pp)$	$C_F^\phi(pn)$
$\phi = \sigma, \omega$	1	1	1	0
$\phi = \delta, \rho, \pi$	1	−1	1	2

$$E_F^{\omega}(u_{p\omega}, u_{n\omega}) = -\frac{3g_\omega^2 m_\omega}{128\pi^2 u_\omega^3}\left[f_3(u_{p\omega}, u_{n\omega}) - \frac{1}{2}\left(\frac{m_\omega}{M}\right)^2 [f_1(u_{p\omega}, u_{n\omega}) - f_3(u_{p\omega}, u_{n\omega}) + f_4(u_{p\omega}, u_{n\omega})] + \frac{1}{4}\left(\frac{m_\omega}{M}\right)^4 [2f_2(u_{p\omega}, u_{n\omega}) - f_4(u_{p\omega}, u_{n\omega})]\right],$$

$$E_F^{\rho}(u_{p\rho}, u_{n\rho}) = -\frac{3g_\rho^2 m_\rho}{128\pi^2 u_\rho^3}\left[f_3(u_{p\rho}, u_{n\rho}) - \frac{1}{2}\left(\frac{m_\rho}{M}\right)^2 [f_1(u_{p\rho}, u_{n\rho}) - f_3(u_{p\rho}, u_{n\rho}) + f_4(u_{p\rho}, u_{n\rho})] + \frac{1}{4}\left(\frac{m_\rho}{M}\right)^4 \times [2f_2(u_{p\rho}, u_{n\rho}) - f_4(u_{p\rho}, u_{n\rho})]\right] + \frac{9g_\rho f_\rho m_\rho}{256\pi^2 u_\rho^3}\left[\left(\frac{m_\rho}{M}\right)^2 [f_1(u_{p\rho}, u_{n\rho}) - f_3(u_{p\rho}, u_{n\rho})] - \frac{1}{2}\left(\frac{m_\rho}{M}\right)^4 \times [2f_2(u_{p\rho}, u_{n\rho}) - f_4(u_{p\rho}, u_{n\rho})]\right] + \frac{3f_\rho^2 m_\rho}{256\pi^2 u_\rho^3}\left[\left(\frac{m_\rho}{M}\right)^2 [f_1(u_{p\rho}, u_{n\rho}) - f_3(u_{p\rho}, u_{n\rho})] - \frac{1}{2}\left(\frac{m_\rho}{M}\right)^4 \times [2f_2(u_{p\rho}, u_{n\rho}) - f_4(u_{p\rho}, u_{n\rho})]\right],$$

$$E_F^{\pi}(u_{p\pi}, u_{n\pi}) = \frac{3f_\pi^2 m_\pi}{128\pi^2 u_\pi^3}\left[[f_1(u_{p\pi}, u_{n\pi}) - f_3(u_{p\pi}, u_{n\pi})] - \frac{1}{2}\left(\frac{m_\pi}{M}\right)^2 [2f_2(u_{p\pi}, u_{n\pi}) - f_4(u_{p\pi}, u_{n\pi})]\right]. \tag{24}$$

The functions, $f_1(u_{p\phi}, u_{n\phi}) \sim f_5(u_{p\phi}, u_{n\phi})$ in Eq. (24) are defined as

$$f_1(u_{p\phi}, u_{n\phi}) \equiv \tfrac{16}{9} u_{p\phi}^3 u_{n\phi}^3,$$
$$f_2(u_{p\phi}, u_{n\phi}) \equiv \tfrac{8}{15} u_{p\phi}^3 u_{n\phi}^3 \left(u_{p\phi}^2 + u_{n\phi}^2\right),$$

$$
\begin{aligned}
f_3(u_{p\phi}, u_{n\phi}) \equiv\ & 2u_{p\phi}u_{n\phi}\left(u_{p\phi}^2 + u_{n\phi}^2\right) - \tfrac{2}{3}u_{p\phi}u_{n\phi} \\
& + \tfrac{8}{3}\left(u_{p\phi}^3 - u_{n\phi}^3\right)\tan^{-1}[u_{p\phi} - u_{n\phi}] \\
& - \tfrac{8}{3}\left(u_{p\phi}^3 + u_{n\phi}^3\right)\tan^{-1}[u_{p\phi} + u_{n\phi}] \\
& - \left[\tfrac{1}{2}\left(u_{p\phi}^2 - u_{n\phi}^2\right)^2 - \left(u_{p\phi}^2 + u_{n\phi}^2\right) - \tfrac{1}{6}\right] \\
& \times [\ln[1 + (u_{p\phi} + u_{n\phi})^2] \\
& - \ln[1 + (u_{p\phi} - u_{n\phi})^2]], \\
f_4(u_{p\phi}, u_{n\phi}) \equiv\ & \tfrac{2}{9}u_{p\phi}u_{n\phi}\left(9u_{p\phi}^4 + 2u_{p\phi}^2u_{p\phi}^2 + 9u_{n\phi}^4\right) \\
& - \tfrac{18}{5}u_{p\phi}u_{n\phi}\left(u_{p\phi}^2 + u_{n\phi}^2\right) + \tfrac{4}{15}u_{p\phi}u_{n\phi} \\
& + \left[\tfrac{16}{5}\left(u_{p\phi}^5 - u_{n\phi}^5\right) - \tfrac{8}{3}\left(u_{p\phi}^3 - u_{n\phi}^3\right)\right] \\
& \times \tan^{-1}[u_{p\phi} - u_{n\phi}] \\
& + \left[- \tfrac{16}{5}\left(u_{p\phi}^5 + u_{n\phi}^5\right) + \tfrac{8}{3}\left(u_{p\phi}^3 + u_{n\phi}^3\right)\right] \\
& \times \tan^{-1}\left[u_{p\phi} + u_{n\phi}\right] \\
& - \left[\tfrac{1}{2}\left(u_{p\phi}^2 + u_{n\phi}^2\right)\left(u_{p\phi}^2 - u_{n\phi}^2\right)^2\right. \\
& \left. - 2\left(u_{p\phi}^4 + u_{n\phi}^4\right) + \tfrac{1}{2}\left(u_{p\phi}^2 + u_{n\phi}^2\right) + \tfrac{1}{15}\right] \\
& \times \left(\ln\left[1 + \left(u_{p\phi} + u_{n\phi}\right)^2\right]\right. \\
& \left. - \ln\left[1 + \left(u_{p\phi} - u_{n\phi}\right)^2\right]\right], \\
f_5(u_{p\phi}, u_{n\phi}) \equiv\ & u_{p\phi}^3u_{n\phi}^3\left(\tfrac{2}{7}u_{p\phi}^4 + \tfrac{4}{25}u_{p\phi}^2u_{n\phi}^2 + \tfrac{2}{7}u_{n\phi}^4\right). \qquad (25)
\end{aligned}
$$

IV. POINT COUPLING TERMS

Based on the expressions (24) for the binding energy which, so far, includes only OME terms we first tried to obtain a reasonable EOS using the density-dependent meson parameters obtained in Ref. [21], which reproduce rather well the behavior of the G-matrix at intermediate and large distances. However, within such an approach, it turned out to be impossible to find satisfactory saturation properties. Because of the large cancellations between repulsive and attractive effects from the Lagrangian, there are many sets of parameters giving almost equal fitting to the G-matrix potentials but producing different results for other relevant quantities. Thus, in the next step, we tried to adjust the parameters of the Lagrangian (1) in such a way that they reproduce the G-matrix potentials at intermediate distances and simultaneously an appropriate EOS for symmetric nuclear matter. Again it remains impossible to obtain satisfactory saturation properties because of the large uncertainties in the short-range behavior of the G-matrix potentials. The short-range part plays an important role in the process of saturation and it is obviously not reproduced properly by the OME form of the potentials in our model. When comparing the G-matrix potentials with OME potentials, we neglect as in Ref. [21] the region of small distances, typically, $r < 0.8$ fm. However, in the calculation of the energy per particle in nuclear matter, the information originating from this region is included. Therefore we cannot find a parameter set to reproduce simultaneously the nuclear matter energy and the G-matrix potentials. In addition it is not fully clear whether the G-matrix itself provides a reasonable description of the effective force at short distances, i.e., for typically $r < 0.8$ fm.

We therefore introduce the following additional coupling terms describing the short-range corrections:

$$
\begin{aligned}
\mathcal{L}_{\rm PC} =\ & -\alpha_\sigma(\bar\psi\psi)^2 - \alpha_\omega(\bar\psi\gamma^\mu\psi)^2 \\
& - \alpha_\delta(\bar\psi\vec\tau\psi)^2 - \alpha_\rho(\bar\psi\gamma^\mu\vec\tau\psi)^2 \qquad (26)
\end{aligned}
$$

and add them to the Lagrangian of finite range interactions in Eq. (1). These terms in Eq. (26) are supposed to represent various effects at small distances which cannot be renormalized into the density-dependent OME part of the Lagrangian. The total Lagrangian thus takes the form

$$
\mathcal{L} = \mathcal{L}_{\rm OME} + \mathcal{L}_{\rm PC}. \qquad (27)
$$

Since there is no detailed knowledge about the physical origin of this short-range part, we use a point coupling ansatz and adjust it to chiral perturbation theory. In Ref. [4], it has been shown by chiral perturbation theory (ChPT) that the short-range contributions to the energy per particle depend mainly on a cut-off parameter Λ. The diverging part of the energy per particle has the form

$$
\begin{aligned}
\bar E_\Lambda(k_f, k_f) = \frac{1}{12\pi^2}\big[&(-15A(\Lambda) + 3B(\Lambda))u_\pi^3 \\
&+ (C(\Lambda) + D(\Lambda))u_\pi^5\big] \qquad (28)
\end{aligned}
$$

for symmetric nuclear matter and

$$
\bar E_\Lambda(0, k_n) = \frac{1}{12\pi^2}\big[(-A(\Lambda) - B(\Lambda))u_{n\pi}^3 + C(\Lambda)u_{n\pi}^5\big], \qquad (29)
$$

for pure neutron matter. The functions $A(\Lambda)$, $B(\Lambda)$, $C(\Lambda)$, and $D(\Lambda)$ are defined as

$$
\begin{aligned}
A(\Lambda) &= \frac{1}{32\pi^2}g_A^4\frac{m_\pi^3 M\Lambda}{f_\pi^4}, \\
B(\Lambda) &= \frac{1}{64\pi^2}\left(3g_A^2 + 1\right)\left(g_A^2 - 1\right)\frac{m_\pi^3\Lambda^2}{f_\pi^4} \\
&\quad - \frac{1}{64\pi^2}\left(-15g_A^4 + 6g_A^2 + 1\right)\frac{m_\pi^5}{f_\pi^4}\ln\left[\frac{m_\pi}{2\Lambda}\right], \qquad (30) \\
C(\Lambda) &= \frac{1}{320\pi^2}\left(-13g_A^4 - 10g_A^2 - 1\right)\frac{m_\pi^5}{f_\pi^4}\ln\left[\frac{m_\pi}{2\Lambda}\right], \\
D(\Lambda) &= \frac{1}{160\pi^2}\left(23g_A^4 - 10g_A^2 - 1\right)\frac{m_\pi^5}{f_\pi^4}\ln\left[\frac{m_\pi}{2\Lambda}\right].
\end{aligned}
$$

Here, g_A is the nucleon axial vector coupling constant with a value, $g_A = 1.26$, and f_π is the weak pion decay constant, $f_\pi = 92.4$ MeV.

The contribution to the energy in nuclear matter calculated from the Lagrangian (26) has, in a nonrelativistic expansion up to forth order in k_f/M, the form

$$
\begin{aligned}
\bar E_{\rm PC}(k_p, k_n) = \frac{m_\pi^3}{24\pi^2u_\pi^3}\Big[&(2\alpha_\sigma + 2\alpha_\omega + 2\alpha_\delta \\
&+ 2\alpha_\rho)\left(u_{p\pi}^6 + u_{n\pi}^6\right) \\
&+ (8\alpha_\sigma + 8\alpha_\omega - 16\alpha_\delta - 16\alpha_\rho)u_{p\pi}^3u_{n\pi}^3
\end{aligned}
$$

$$
\begin{aligned}
&- \frac{3}{5}\left(\frac{m_\pi}{M}\right)^2 (3\alpha_\sigma - 4\alpha_\omega + 3\alpha_\delta \\
&- 4\alpha_\rho)\left(u^8_{p\pi} + u^8_{n\pi}\right) \\
&- \frac{3}{5}\left(\frac{m_\pi}{M}\right)^2 (4\alpha_\sigma - 6\alpha_\delta - 8\alpha_\rho) u^3_{p\pi} u^3_{n\pi} \\
&\times \left(u^2_{p\pi} + u^2_{n\pi}\right)\Bigg]. \qquad (31)
\end{aligned}
$$

Comparing Eq. (31) with Eqs. (28) and (29), we see that they become identical, if we choose our parameters as

$$
\begin{aligned}
\alpha_\sigma(\Lambda) &= \frac{1}{m_\pi^3}\left[\frac{30}{7}A - \frac{12}{7}B - \left(\frac{M}{m_\pi}\right)^2\left(\frac{5}{6}C - \frac{5}{21}D\right)\right], \\
\alpha_\omega(\Lambda) &= \frac{1}{m_\pi^3}\left[-\frac{81}{14}A + \frac{12}{7}B + \left(\frac{M}{m_\pi}\right)^2\left(\frac{5}{6}C - \frac{5}{21}D\right)\right], \\
\alpha_\delta(\Lambda) &= \frac{1}{m_\pi^3}\left[-\frac{32}{7}A + \frac{10}{7}B + \left(\frac{M}{m_\pi}\right)^2\left(\frac{5}{6}C - \frac{10}{21}D\right)\right], \\
\alpha_\rho(\Lambda) &= \frac{1}{m_\pi^3}\left[\frac{39}{7}A - \frac{27}{14}B - \left(\frac{M}{m_\pi}\right)^2\left(\frac{5}{6}C - \frac{10}{21}D\right)\right]. \qquad (32)
\end{aligned}
$$

In the following, we adopt this choice for the parameters $\alpha_\sigma \ldots \alpha_\rho$. Finally we obtain, for the energy derived from the point coupling Lagrangian (26), the following expression:

$$
\begin{aligned}
\bar{E}_{\rm PC}(k_p, k_n) = \frac{1}{24\pi^2 u_\pi^3}\big[&- (A(\Lambda) + B(\Lambda))\left(u^6_{p\pi} + u^6_{n\pi}\right) \\
&- (28A(\Lambda) - 8B(\Lambda)) u^3_{p\pi} u^3_{n\pi} \\
&+ C(\Lambda)\left(u^8_{p\pi} + u^8_{n\pi}\right) \\
&+ D(\Lambda) u^3_{p\pi} u^3_{n\pi}\left(u^2_{p\pi} + u^2_{n\pi}\right)\big]. \qquad (33)
\end{aligned}
$$

It contains only one free parameter Λ which does not depend on the density. It will be determined by adjusting to the energy per particle of symmetric nuclear matter as a function of the density in the next section.

Schiller and Müther [27] used a different way to take into account the effects of many-body correlations in the nuclear medium. They decomposed the G-matrix $G = V + \Delta G$ into the bare interaction V and a term ΔG, which takes into account the correlations in the many-body system. ΔG is parametrized as a meson-exchange with very heavy mesons by zero range forces and the coupling constants in the four spin-isospin channels are adjusted to the G-matrix.

V. THE DETERMINATION OF THE PARAMETERS OF THE MODEL

In this section, we discuss the choice of the parameters included in the present model. These are the masses $m_\phi(\rho)$ and the coupling constants $g_\phi(\rho)$ of the four mesons $\phi = \sigma, \delta, \omega$, and ρ, which depend on the density and the cutoff-parameter Λ in the point coupling part $\mathcal{L}_{\rm PC}$. Note that Λ does not depend on the density. For the pion we adopt the bare values, i.e $m_\pi = 137.0$ MeV and $f_\pi^2/4\pi = 0.081$ for the mass and the coupling constant. The tensor coupling for the ρ-meson is kept fix at $f_\rho/g_\rho = 6.10$, a value determined from the $\pi\pi \to N\bar{N}$ partial wave dispersion analysis of Ref. [28].

TABLE II. Ranges of the G-matrix potentials used for the fitting in units of fm.

V_0:	$0.8 < r < 2.0$
V_σ:	$1.2 < r < 2.0$
V_τ:	$0.8 < r < 2.0$
$V_{\sigma\tau}$:	$1.1 < r < 2.0$
V_{ls}:	$0.8 < r < 2.0$
$V_{\rm tensor}$:	$0.6 < r < 2.0$

We determined the parameters $m_\phi(\rho)$ and the coupling constants $g_\phi(\rho)$ at the densities given by the Fermi momenta $k_f = 1.0$, 1.2, 1.4, 1.6, 1.8, and 2.0 fm^{-1} by fitting the radial dependence of the OME-potentials to the G-matrix potentials. The ranges used for the fit are given in Table II. Table II clearly indicates that only intermediate- and long-distance properties of NN interactions are included in the fit. It turns out that the σ-meson depends very weakly on the density. The parameters of the δ-meson increase gradually, and those for the ω- and ρ-meson decrease slowly as the density increases. As discussed in the previous section, in this work we determine the meson parameters (and the cutoff parameter Λ) not only adjusting to the G-matrix potentials, but also to the EOS of symmetric nuclear matter. For that purpose we need an analytic expression for the density dependence of the meson-parameters. In order to reproduce the features found in Ref. [21] we choose the following functional form:

$$
\begin{aligned}
g_\phi(k_f) &= \tfrac{a}{k_f}\ln\left[b^2 k_f^2 + 1\right] + c, \\
m_\phi(k_f) &= \tfrac{a}{k_f}\ln\left[b^2 k_f^2 + 1\right] + c, \qquad (34)
\end{aligned}
$$

which contain for each meson six parameters a, b, and c (three for the coupling g and three for the mass m). Note that a for g and a for m are different and independent. Assuming this form for the density dependence, we adjust the 24 parameters a, b, c and the density independent cutoff parameter Λ for each density in such a way that at each density ($k_f = 1.0$, 1.2, 1.4, 1.6, 1.8, and 2.0 fm^{-1}):

(i) the OME potentials reproduce the radial dependence of the G-matrix potentials in the ranges given in Table II and
(ii) the energy per particle for symmetric nuclear matter calculated with the full Lagrangian (27) reproduces the value of the EOS calculated with the Gogny force GT2 derived in Refs. [29,30].

The GT2 interaction, which we choose as a guideline, is an improved Gogny-type interaction with some changes, e.g., the inclusion of a tensor interaction. The GT2 interaction reproduces the isospin dependence of shell structures [29,30] more precisely. Thus this interaction is suitable for the study of exotic nuclei, while its EOS does not differ from the one obtained from the D1S interaction [31] for symmetric nuclear matter. Note that we used GT2 rather than D1S, because the

TABLE III. Parameters of the present model. The parameters, a, b, and c describe the density dependence as defined in Eq. (34).

	a	b	c
m_σ	62.129	1.3274	420.298
m_ω	−1337.38	0.3083	883.319
m_δ	928.809	1.1301	430.616
m_ρ	−1211.25	0.2924	856.712
g_σ	39.435	0.0019	10.193
g_ω	−18.774	0.4256	17.692
g_δ	50.700	0.3828	3.823
g_ρ	−16305.8	0.0031	2.903
f_ρ/g_ρ	–	–	6.10
m_π	–	–	137.0
$f_\pi/4\pi^2$	–	–	0.081
M	–	–	939.0
Λ	–	–	300.832

former produces a better result for the incompressibility than the latter.

The parameters a, b, and c in Eq. (34) found in this investigation are shown in Table III. The parameters, $f_\rho/g_\rho, m_\pi, f_\pi/4\pi^2$, and M are fixed to the values listed in the table. The cutoff Λ is treated as a free parameter. However, it has no density dependence. The results for the density dependence of the masses and the coupling constants of the mesons are shown in Figs. 5 and 6. The density dependencies of the ω and ρ meson mass are very similar. Both masses decrease with increasing density. This tendency is consistent with requirements of chiral symmetry and QCD oriented models [32–34]. What is practical between the present model and other DDRMF models [13–15] is the fact that the density dependence of the parameters of the present model is weaker. The origin for this is the inclusion of the point coupling interactions. As discussed in Sec. VII, the present model produces a softer EOS than other RMF models [35] due to the decrease of the vector meson parameters and the weak density dependence of the σ meson. The parameters of the present model are also consistent with other RMF models at the saturation point. These values at the saturation density $k_{f0} = 1.35$ fm^{-1} (which corresponds to $\rho_0 = 0.165$ fm^{-3}) are listed in Table IV. For comparison we list also the parameters of some RMF models [7–9], with nonlinear meson-couplings and with density dependent coupling constants [15]. Many parameters are almost the same as the corresponding ones in these RMF models. However, in the present model, g_ρ is apparently smaller than that in the other RMF models. The reason for this difference is that we have included also the δ meson as well as a tensor term for the ρ meson in the model. This is not the case in the other models, where the isospin dependence is carried by the ρ meson alone.

The cutoff parameter Λ becomes $\Lambda = 300.8$ MeV. This value is considerably lower than the value of $\Lambda = 646.3$ MeV adopted in the model of Ref. [4] based on chiral perturbation theory. However, in our calculation, the point coupling contribution added in the Lagrangian $\mathcal{L}_{\rm PC}$ in Eq. (26) is not necessarily equal to the full short-range contribution. The short-range contribution from the OME part is rather sizable. It deviates considerably from the short-range contribution of the G-matrix and the point coupling part works as a correction to the short-range contribution of the OME part. This is the reason for the difference between the cutoff parameter Λ of the present model and the cutoff scale of chiral perturbation theory obtained in Ref. [4].

In Fig. 7 we show the radial dependencies of the OME for the density with $k_f = 1.4$ fm^{-1}. The results at $k_f = 1.0$ fm^{-1} and $k_f = 1.8$ fm^{-1} are vary similar. At each density the OME potentials are in good agreement with the G-matrix potentials. It turns out to be very important to introduce the isovector mesons (π and δ), and the tensor coupling of the ρ meson in order to reproduce the potentials $\mathcal{V}_\tau(r)$ and $\mathcal{V}_T(r)$. All these terms depend on isospin and therefore we expect that these terms play a crucial role for the description of

TABLE IV. Comparison for the parameters between the present model and four RMF models [7–9, 15]. The meson masses and the coupling constants are density dependent in our model we therefore give the values at the point of saturation. The cutoff parameter Λ does not depend on the density.

Parameter	present model ($k_{f0} = 1.35$ fm^{-1})	NL1	NL-SH	NL3	DD-ME2
M [MeV]	939.0	938.0	939.0	939.0	939.0
m_σ [MeV]	486.450	492.25	526.059	508.194	550.1238
m_δ [MeV]	1257.310	–	–	–	–
m_π [MeV]	137.0	–	–	–	–
m_ω [MeV]	725.467	795.359	783.0	782.501	783.0
m_ρ [MeV]	727.128	763.0	763.0	763.0	763.0
g_σ	10.193	10.138	10.444	10.217	10.5396
g_δ	12.688	–	–	–	–
$\frac{f_\pi^2}{4\pi}$	0.081	–	–	–	–
g_ω	13.735	13.285	12.945	12.868	13.0189
g_ρ	2.698	4.976	4.383	4.474	3.6836
$\frac{f_\rho}{g_\rho}$	6.10	–	–	–	–
Λ [MeV]	300.8	–	–	–	–

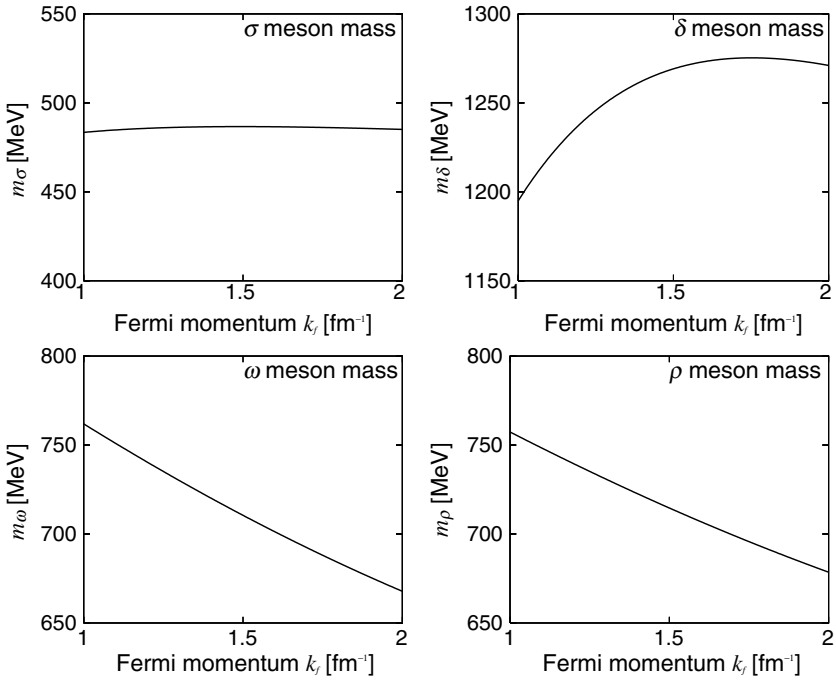

FIG. 5. Density dependence of each meson mass. From the left to the right and from the top to the bottom, the pictures represent the density dependence of $m_\sigma, m_\delta, m_\omega$, and m_ρ, respectively.

isospin properties of nuclei far from the valley of stability. In fact, the importance of these terms has been already found in a study within the shell model. The significant change of the shell structures, called *shell evolution*, has been presented as a result of the spin-isospin interaction [36–39]. The same scenario can be applied in the case of nonrelativistic Hartree-Fock calculation [29,30]. From such discussions, it is very interesting to treat the tensor interaction explicitly. In the case of RMF models this tensor interaction enters into the Fock term of the derivative coupling of the π meson and of the tensor coupling of the ρ meson. Therefore it seems to be important to take into account these terms in the present model.

VI. NUCLEAR MATTER PROPERTIES

We now apply our model to the calculation of properties of nuclear matter. First we concentrate on symmetric nuclear matter. Figure 8 shows the energy per particle as a function of the density calculated by three different methods. The full line

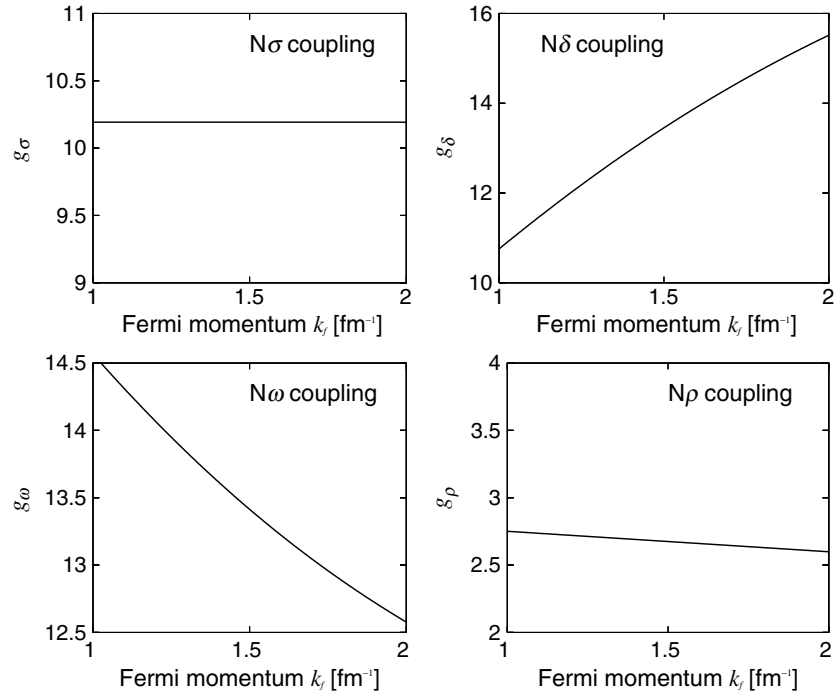

FIG. 6. Density dependence of each meson-nucleon coupling. From left to right and from top to bottom, the pictures represent the density dependence of $g_\sigma, g_\delta, g_\omega$, and g_ρ, respectively.

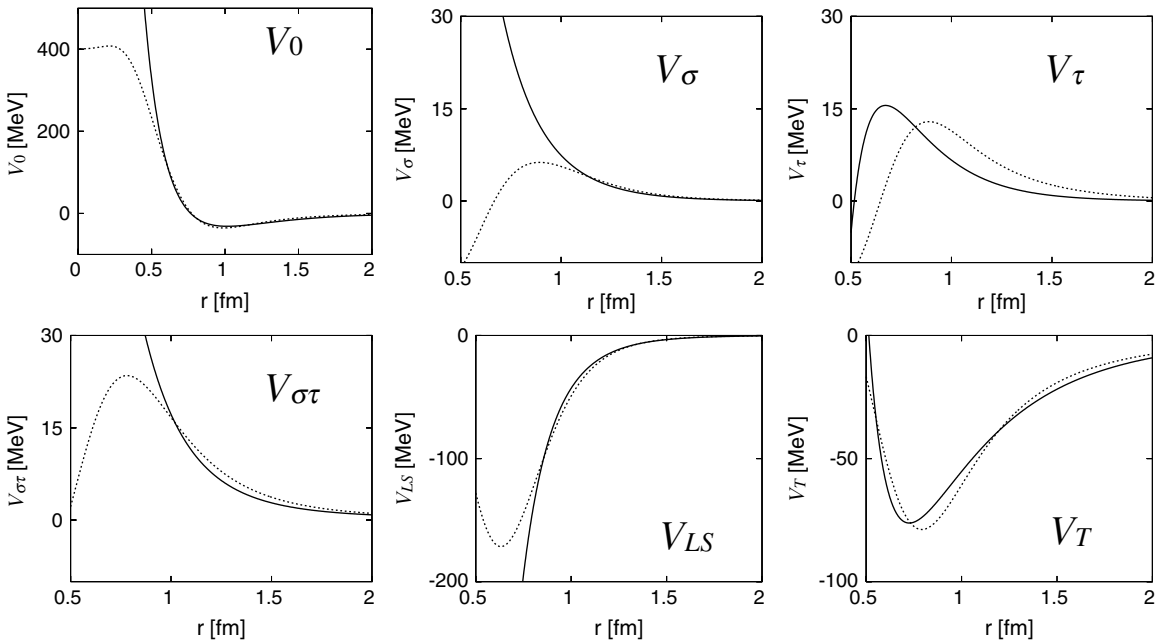

FIG. 7. G-matrix potentials and OME potentials at the density $k_f = 1.4$ fm^{-1}. From left to right and from top to bottom, the pictures represent the potential of each channel, $\mathcal{V}_0$, $\mathcal{V}_\sigma$, $\mathcal{V}_\tau$, $\mathcal{V}_{\sigma\tau}$, $\mathcal{V}_{\rm LS}$, and $\mathcal{V}_T$, respectively. The solid line represents OME potentials and dotted line represents G-matrix potentials (Akaishi potential).

corresponds to the results derived within the present model obtained by the method discussed in Sec. III. It is compared with the energy per particle based on the modified Gogny force GT2 calculated in Ref. [40] and with results derived from the G-matrix potentials discussed in Fig. 3. Obviously the latter case shows no saturation within the given density range. There are two reasons for this shortcoming. First it is well known, that in nonrelativistic calculations without three-body forces the saturation is achieved only at considerably larger densities [41]. In addition we have taken into account in the G-matrix only the density dependence arising from the Pauli projector. We neglected in our calculations the density dependence of the G-matrix entering through the self-consistent treatment of the starting energy. At densities relevant for this investigation this second density dependence is rather weak. However, it becomes important at large densities, and so its neglect prevents nuclear saturation in the density region shown in Fig. 8.

The result for the energy per particle of our present model is almost identical to that of the Gogny force GT2, because this case has been used in order to adjust the parameters. However, it is not trivial and it is, indeed, very important that we reproduce simultaneously the energy per particle and the radial dependence of the G-matrix potentials in the range of typically $r > 0.8$ fm. The saturation point is $k_{f0} = 1.35$ fm^{-1} (which corresponds to $\rho_0 = 0.165$ fm^{-3}), and the saturation energy is $\bar{E}(k_{f0}, k_{f0}) = 16.2$ MeV. The nuclear incompressibility K is related to the curvature at the minimum. We find

$$K = k_{f0}^2 \frac{\partial^2 \bar{E}(k_f, k_f)}{\partial k_f^2}\bigg|_{k_f = k_{f0}} = 241 \text{ MeV}.$$

This value is in agreement with the most recent relativistic and nonrelativistic investigations based on the experimental breathing mode energies in finite nuclei, which find $K = 250 \pm 25$ MeV [5,42,43].

In Table V we show the contributions to the energy per particle coming from the various mesons and from the point coupling part of the Lagrangian at the saturation point. From this table, we see that it is possible to reproduce G-matrix potentials and saturation energy simultaneously by models in which only σ and ω meson are included, if we neglect the channels which carry isospin. Namely, at the saturation density, $\bar{E}_{\rm kin} + \bar{E}_\sigma + \bar{E}_\omega = -9.8$ MeV is in the same order of magnitude as $\bar{E}(k_{f_0}, k_{f_0}) = -16.2$ MeV. On the other hand, it is difficult to reproduce them simultaneously when we take into account the channels carrying isospin. The reason for this

TABLE V. Contribution from each meson and point coupling part to the energy of isospin-symmetric nuclear matter at the saturation density ($k_{f0} = 1.35$ fm^{-1}). The kinetic energy at the saturation density is $\bar{E}_{\rm kin} = 22.2$ MeV.

	Attraction	Repulsion	Total
$T = 0$	$\bar{E}_\sigma = -214.4$ MeV	$\bar{E}_\omega = 182.4$ MeV	-32.0 MeV
$T = 0, T = 1$	$\bar{E}_{\rm PC} = -78.0$ MeV	$\bar{E}_\delta + \bar{E}_\pi + \bar{E}_\rho = 71.6$ MeV	-6.4 MeV

TABLE VI. Contributions from Hartree and Fock terms of mesons and from the point coupling part to the energy per particle in isospin-symmetric nuclear matter at the density $k_f = 1.35$ fm^{-1} ($\rho = 0.165$ fm^{-3}) (left) and $k_f = 1.80$ fm^{-1} ($\rho = 0.394$ fm^{-3}) (right). The energies are given in units of MeV.

$k_f = 1.35$	Hartree	Fock	Total	$k_f = 1.80$	Hartree	Fock	Total
$\bar{E}_{\rm kin}$	–	–	22.2	$\bar{E}_{\rm kin}$	–	–	39.3
$\bar{E}_{\sigma}$	−265.7	51.3	−214.4	$\bar{E}_{\sigma}$	−614.9	102.6	−512.3
$\bar{E}_{\delta}$	0.0	44.9	44.9	$\bar{E}_{\delta}$	0.0	133.2	133.2
$\bar{E}_{\pi}$	0.0	18.3	18.3	$\bar{E}_{\pi}$	0.0	46.5	46.5
$\bar{E}_{\omega}$	227.2	−44.9	182.4	$\bar{E}_{\omega}$	537.2	−87.9	449.4
$\bar{E}_{\rho}$	0.0	8.4	8.4	$\bar{E}_{\rho}$	0.0	39.1	39.1
$\bar{E}_{\rm PC}$	−54.6	−23.4	−78.0	$\bar{E}_{\rm PC}$	−130.5	−60.0	−190.5
Total	−93.0	54.6	−16.2	Total	−208.1	173.5	4.8

difficulty is the too strong repulsion generated by the δ, π, and ρ mesons which carry isospin. Therefore, it is necessary to introduce the point coupling terms into the model. As shown in Table V, there is nearly perfect cancellation of the large repulsive terms originating from the mesons carrying isospin and the attractive term resulting from the point coupling interaction. Therefore it becomes possible to reproduce the G-matrix potentials and the saturation energy simultaneously, even with the mesons carrying isospin. Thus, it is necessary to introduce point coupling terms, when we want to treat the isospin dependence introduced by the various mesons correctly.

The contribution to the energy per particle in isospin-symmetric nuclear matter and pure neutron matter are shown in Tables VI and VII for Hartree and Fock terms. From these tables and figures one can deduce a few important facts: First, we cannot neglect Fock terms. For the σ and ω channels the Fock terms are smaller than the Hartree terms and there is also the usual cancellation between attractive σ contributions and repulsive ω contributions. However for the other three channels with isospin (δ, π, and ρ) the Hartree term vanishes because of isospin symmetry and the Fock terms contribute with the same sign. Therefore, the total contribution from the Fock terms becomes sizable compared with Hartree terms. Of course the tensor terms do not contribute in these tables because of spin-saturation of nuclear matter.

Fock terms become more important with increasing density. From the tables, we see that the sum of the Fock terms increases more rapidly than that of the Hartree terms decreases, and the slope becomes steeper than that of the Hartree contributions. Therefore, the total energy becomes more repulsive as the density increases. In the present model, this rapid increase of Fock terms plays an important role for reproducing the saturation mechanism.

We also calculate the asymmetry energy in the present model. Expanding the energy per particle of isospin-asymmetric nuclear matter $\bar{E}(\rho, \alpha)$ in Eq. (14) in powers of α around $\alpha = 0$,

$$\bar{E}(\rho, \alpha) = \bar{E}(\rho, 0) + \alpha^2 S_2(\rho) + \cdots \tag{35}$$

the asymmetry energy $S(\rho)$ is defined as the coefficient of α^2:

$$S_2(\rho) = \frac{1}{2}\frac{\partial^2}{\partial \alpha^2}\bar{E}(\rho, \alpha)\bigg|_{\alpha=0}. \tag{36}$$

Note that the parameter α is equal to $(\rho_n - \rho_p)/(\rho_n + \rho_p) = (N - Z)/(N + Z)$. The result is shown in Fig. 9, where we compare the density dependence of the asymmetry energy of the present model with that of the G-matrix potential and with that of the DDRMF model. We find that our model is in nearly perfect agreement with the curve obtained with the parameter set DD-ME1 of Ref. [14].

TABLE VII. Contributions from Hartree and Fock terms of mesons and from the point coupling part to the energy per particle in the pure neutron matter at the density $k_f = 1.35$ fm^{-1} ($\rho = 0.165$ fm^{-3}) (left) and $k_f = 1.80$ fm^{-1} ($\rho = 0.394$ fm^{-3}) (right). The energies are given in units of MeV.

$k_f = 1.35$	Hartree	Fock	Total	$k_f = 1.80$	Hartree	Fock	Total
$\bar{E}_{\rm kin}$	–	–	35.0	$\bar{E}_{\rm kin}$	–	–	61.4
$\bar{E}_{\sigma}$	−259.0	89.4	−169.5	$\bar{E}_{\sigma}$	−589.8	168.1	−421.7
$\bar{E}_{\delta}$	−60.1	28.6	−31.5	$\bar{E}_{\delta}$	−179.8	82.0	−97.8
$\bar{E}_{\pi}$	0.0	12.9	12.9	$\bar{E}_{\pi}$	0.0	31.1	31.1
$\bar{E}_{\omega}$	227.2	−79.2	148.0	$\bar{E}_{\omega}$	537.2	−142.4	394.8
$\bar{E}_{\rho}$	8.7	9.6	18.3	$\bar{E}_{\rho}$	21.9	37.0	58.8
$\bar{E}_{\rm PC}$	−9.2	13.8	4.6	$\bar{E}_{\rm PC}$	−22.0	53.7	31.7
Total	−92.3	75.1	17.8	Total	−232.4	229.4	58.4

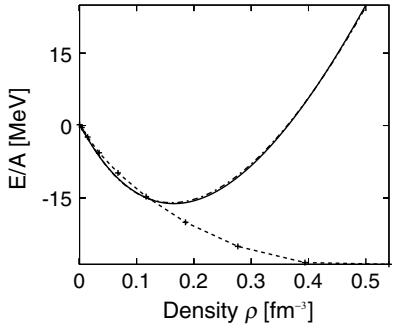

FIG. 8. Energy per particle for isospin-symmetric nuclear matter. Results of the present model (solid line) are compared with those of the G-matrix potentials (dashed line) and those of the GT2-interaction Refs. [29,30] (dashed-dotted line).

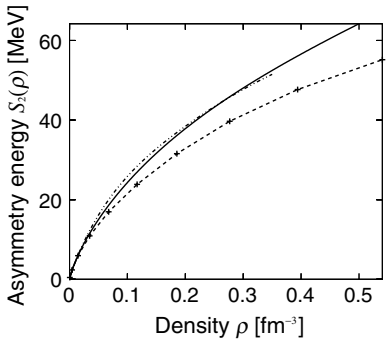

FIG. 9. Symmetry energy of the present model (solid line) compared with results of the G-matrix potentials (dashed line) and with those of the density dependent RMF parameter set DD-ME1 of Ref. [14] (dashed-double-dotted line).

The asymmetry energy of the G-matrix potentials shows deviations, in particular it increases less with density than the other two curves. We find for the asymmetry energy at saturation a value of $S_2(\rho_{\text{sat}}) \approx 30$ MeV. The close agreement of the results obtained with our model and with the fully phenomenologically determined parameter set DD-ME1 is surprising. This results is not obtained by a fit to experimental data on nuclei with mass asymmetry. Our fit contains only information on the scattering data and on the EOS for symmetric nuclear matter.

The symmetry energy is often approximated by a polynomial around the saturation point

$$S_2(\rho) = a_4 + \frac{p_0}{\rho_{\text{sat}}^2}(\rho - \rho_{\text{sat}}) + \frac{\Delta K_0}{18\rho_{\text{sat}}^2}(\rho - \rho_{\text{sat}})^2 \ldots, \qquad (37)$$

where a_4 is the asymmetry energy at saturation. We find in our model $a_4 = S_2(\rho_{\text{sat}}) = 33.6$ MeV. This value is in good agreement with the empirical value of $S_2(\rho_{\text{sat}}) = 33.2$ MeV obtained in Ref. [44] from extensive and elaborate fitting to nuclear masses. The parameter p_0 defines the slope of the symmetry energy curve at saturation and the parameter ΔK_0 is the curvature. It contributes to the incompressibility of asymmetric nuclear matter. In Table VIII we compare our results for these values with other relativistic models. The nonlinear effective interactions NL1 and NL3 have considerably larger values for a_4. This has its origin in the fact that these sets have no density dependence in the channel carrying isospin, i.e., in the ρ channel. In a recent analysis of neutron radii in finite nuclei Furnstahl [45] has shown that the empirical value of $r_n - r_p$ in ^{208}Pb (0.20 ± 0.04 fm from proton scattering data [46], and 0.19 ± 0.09 fm from the alpha scattering excitation of the isovector giant dipole resonance [47]) places the following constraints on the values of the parameters of the symmetry energy: $a_4 \approx 30$–34 MeV, $2\ \text{MeV/fm}^3 \leqslant p_0 \leqslant 4\ \text{MeV/fm}^3$, and $-200\ \text{MeV} \leqslant \Delta K_0 \leqslant -50$ MeV. From Table VIII we see that these constraints are satisfied by our model and by the density-dependent model DD-ME1, but not by the models NL1 and NL3, which do not have a density dependence in the isospin ρ channel.

TABLE VIII. Parameters characterizing the asymmetry $S_2(\rho)$ for various parameter sets DD-ME1 [14], NL1 [7], and NL3 [8].

	present model	DD-ME1	NL1	NL3
a_4 [MeV]	33.6	33.1	43.7	37.9
p_0 [MeV fm^{-3}]	3.46	3.26	7.0	5.92
ΔK_0 [MeV]	−106.9	−128.5	67.3	52.1

The extreme case of asymmetric nuclear matter is the pure neutron matter. All existing realistic calculations [23,48–50] agree that pure neutron matter is unbound and its energy per particle increases monotonically as the neutron density increases. The results for the energy per particle of the pure neutron matter is shown in Fig. 10. It shows also the results of the many-body calculations of the Urbana group [23]. This curve should be considered as representative of most of the existing neutron matter calculations [48–50] which scatter around it. Our result is in rather good agreement with that of the Urbana group. The parameter set DD-ME1 reproduces these results only at smaller densities up to $\rho < 0.2$ fm^{-3}. At higher densities it leads to a stiffer EOS for neutron matter. The GT2 interaction is far from reproducing these results. The

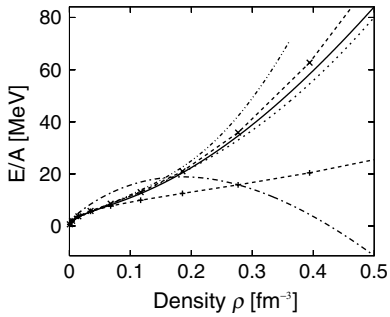

FIG. 10. Energy per particle of pure neutron matter for the present model (solid line), the many-body calculation of Freedman and Phandharipande [23] (dotted line), the density dependent RMF model DD-ME1 of Ref. [14] (dashed-double-dotted line), the modified Gogny interaction of Refs. [29,30] (dashed-dotted line), the pure G-matrix potential (dashed line with + signs), and the G-matrix containing in addition contributions form three-body forces (dashed line with × signs, explained in the text), respectively.

slope of the energy curve of the GT2 interaction becomes negative roughly above saturation density of symmetric nuclear matter.

The results obtained with the G-matrix (dashed curve with + signs in Fig. 10) are also far from the results of the Urbana group, because they do not contain three-body forces. They are, however, in reasonable agreement with the results obtained by the Urbana group for pure two-body interactions shown in Ref. [23]. If one replaces the three-body force used by the Urbana group by an effective two-body interaction [51] one finds a strong repulsive central term for short distances and a tensor term, which causes attraction in symmetric nuclear matter. In pure neutron matter ($T = 1$) this tensor term is very small and the repulsive central term dominates. We have calculated these contributions of the three-body force and after adding them to the results of the pure G-matrix we find the dashed line with × signs in Fig. 10. It is in agreement with the results of the Urbana group (dotted line).

The contribution of Hartree and Fock terms of the OME potentials and of the point coupling part to the energy per particle in the pure neutron matter are shown in Table VII. We see that the energy per particle becomes more repulsive as the density increases by the same mechanism as in the case of isospin-symmetric nuclear matter, namely the rapid increase of the Fock terms. Comparing with the case of isospin-symmetric nuclear matter, the most apparent difference is the sign of the point coupling contribution. They are opposite for symmetric matter and neutron matter. In the case of symmetric matter, the point coupling contribution is attractive. On the other hand, it becomes repulsive in the case of the pure neutron matter. Because of this difference, pure neutron matter becomes unbound at any density while there appears saturation in isospin-symmetric nuclear matter. Therefore, we see that the point coupling part plays an important role for introducing the appropriate isospin dependence into the present model.

In Fig. 11 we show the energy per particle as a function of the density for various values of the asymmetry parameter, given by the Z/N ratio. We find saturation up to rather small proton values of Z/N. However, the saturation density is considerably reduces a smaller values of Z/N. Below a critical values between 10 and 20% protons nuclear matter is no longer bound.

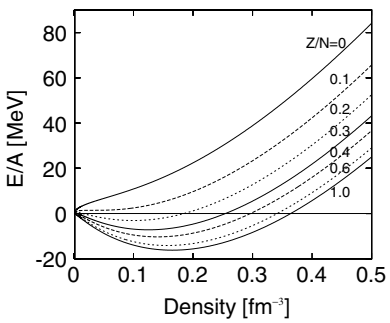

FIG. 11. Energy per particle of nuclear matter as a function of the density for various values of the asymmetry indicated by the Z/N ratio.

VII. APPLICATION TO NEUTRON STARS

In the previous section, we have shown that the present model works well up to $\rho < 3\rho_0$. In this section, we test this model at higher density, applying it directly to densities up to $\rho < 10\rho_0$. For this purpose, we calculate the behavior of neutron stars in the framework of the present model.

A neutron star consists of almost pure neutron matter, and its central density is greater than that of nuclei. Therefore the investigation of its behavior can serve as a test for models studying the properties of dense and relativistic many-body systems.

A. The neutron star model

The structure of a static spherical star is determined by the Oppenheimer-Volkoff-Tolman (OVT) equation [52,53] of general relativity. It has the form

$$\frac{dP}{dr} = -\frac{G\mathcal{M}\epsilon}{r^2}\left(1+\frac{P}{\epsilon}\right)\left(1+\frac{4\pi r^3 P}{\mathcal{M}}\right)\Big/\left(1-\frac{2G\mathcal{M}}{r}\right), \tag{38}$$

$$\frac{d\mathcal{M}}{dr} = 4\pi r^2\epsilon.$$

Here, G is the gravitational constant, $\mathcal{M}(r)$ is the mass contained in a sphere of radius r and $P(r)$ is the pressure at the radius r. The mass can be expressed by the energy density $\epsilon(r)$

$$\mathcal{M}(r) = \int_0^r dx 4\pi x^2 \epsilon(x). \tag{39}$$

The first of the OVT equations describes hydrostatic equilibrium, the second corresponds to the mass balance. The Newtonian form of the first equation is illusive since the space-time is curved. The system of Eqs. (38) is not closed. It needs to be supplemented by an EOS, $\epsilon = \epsilon(\rho)$. Considering that the pressure is given as $P = \rho d\epsilon/d\rho - \epsilon$, we have a closed system of equations for the functions $P(r)$, $\rho(r)$, and $\mathcal{M}(r)$, which can be solved with the boundary condition, that the pressure vanishes at the surface of the neutron star

$$P(R) = 0. \tag{40}$$

Thus, the EOS is a crucial input for structure calculation of neutron stars. In this paper, we use the EOS derived from the present model and apply it directly to the calculation of a neutron star. In the neutron star, $P > 0$ and $dP/dr < 0$. This allows us to determine the total gravitational mass of the star, $\mathcal{M}(R)$.

When calculating neutron star properties, it is necessary to consider not only nucleons but also leptons. Charge-neutral neutron stars include not only neutrons and protons, but also leptons, mainly e^- and μ^- in equal number to protons. Hyperons can also appear at high density. In this section, we neglect hyperons. Nucleons, e^-, and μ^- are taken into account. The Lagrangian for the neutron star has therefore a nuclear part

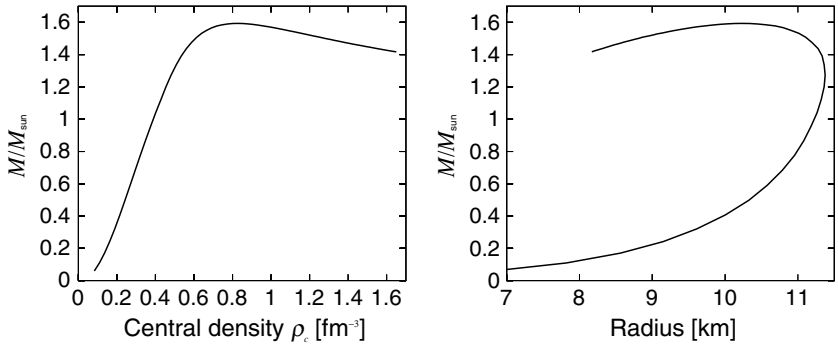

FIG. 12. Neutron star mass is drawn as a function of the central density (left) and the radius (right) of a neutron star.

$\mathcal{L}_{\rm N}$ given by Eq. (27) and leptonic parts $\mathcal{L}_\lambda$:

$$\mathcal{L}_{\rm NS} = \mathcal{L}_{\rm N} + \sum_{\lambda=e^-,\mu^-} \mathcal{L}_\lambda,$$
$$\mathcal{L}_\lambda = \bar{\psi}_\lambda (i\gamma^\mu \partial_\mu - m_\lambda)\psi_\lambda. \tag{41}$$

In order to determine the density of the various particles, we can use the conditions of chemical equilibrium:

$$\mu_p + \mu_e = \mu_n,$$
$$\mu_\mu = \mu_e, \tag{42}$$

where μ_p, μ_n, μ_e, and μ_μ are chemical potentials of proton, neutron, electron, and μ^-, respectively. The chemical potentials of free leptons, μ_λ, are the solutions of their equations of motion:

$$\mu_\lambda = \sqrt{k_\lambda^2 + m_\lambda^2}, \tag{43}$$

where k_λ is the Fermi momentum of each lepton and the density of it is expressed as

$$\rho_\lambda = \frac{k_\lambda^3}{3\pi^2}. \tag{44}$$

Equation (42) expresses that at low density, neutron star matter is composed mostly of neutrons with a few percent admixture of equal number of protons and electrons. If the Fermi energy of electrons exceeds the muon rest energy, $m_\mu = 105.7$ MeV, replaces a fraction of electrons in order to minimize the total energy of the system. In addition baryon number conservation and charge-neutrality conditions are given by

$$\rho = \sum_{\tau=p,n} \rho_\tau = \sum_{\tau=p,n} \frac{k_\tau^3}{3\pi^2},$$
$$Q = Q_p + \sum_{\lambda=e^-,\mu^-} Q_\lambda = \frac{k_p^3}{3\pi^2} - \sum_{\lambda=e^-,\mu^-} \frac{k_\lambda^3}{3\pi^2} = 0. \tag{45}$$

Here $\rho_{p,\lambda}$ and $Q_{p,\lambda}$ represent the density and the electric charge of each particle, and Q is the total electric charge. Using Eqs. (38), (41), (42), and (45), we can calculate the mass and the radius of a neutron star. The result is shown in the next section.

B. Mass and radius of a neutron star

With the present model, we calculate the mass and the radius of a neutron star. Here, we assume that the neutron star matter can be described by the EOS of matter composed of protons, neutron, electrons and muons. We neglect hyperons. In addition, we assume zero temperature and beta equilibrium without trapped neutrinos.

The result for the neutron star mass is drawn in Fig. 12 as a function of the central density ρ_c and as a function of the radius R of a neutron star. The right-hand-side of the first OVT equation describes the gravitational attraction acting on a unit proper-volume of matter. The gravitational pull is given by a Newtonian-like term, $-G\mathcal{M}\epsilon/r^2$, multiplied by three relativistic factors in brackets. As the neutron star mass $\mathcal{M}(R)$ increases, all three factors amplify the attraction compared with the Newtonian case. The increase of $\mathcal{M}(R)$ with an increase of the central pressure $P_c = P(0)$ becomes larger. Therefore, independently of the form of the adopted EOS, there exists always an upper bound on the neutron star mass $\mathcal{M}(R)$ as a consequence of general relativity. In our case we find for the maximal mass

$$\mathcal{M}_{\rm max} = 1.59\mathcal{M}_\odot \quad \text{with} \quad R = 10.29 \text{ km}. \tag{46}$$

The central density for this maximal mass is $\rho_c = 0.832$ fm^{-3} ($\sim 5.0\ \rho_0$). As the central density increases, the mass of the neutron star increases to the maximum mass configuration and then decreases at densities above this point. In the region of $\partial\mathcal{M}(R)/\partial\epsilon(0) < 0$, the neutron star is unstable against a collapse leading to a black hole.

The present model produces an EOS softer than many other RMF models [35]. The neutron star EOS derived from the present model is shown in Fig. 13. Due to the softer EOS, the present model produces a maximum mass which is smaller than that derived from other RMF models. There are two reasons, why our EOS is softer.

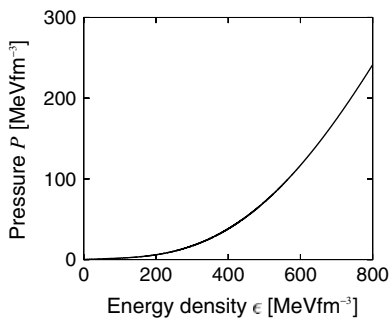

FIG. 13. Equation of state of $npe\mu$ neutron star matter.

(i) The parameters of the vector mesons included in the present model are slowly decreasing with increasing density. Since the vector mesons ω and ρ produce repulsion, their decreasing tendency implies that the repulsion coming from the exchange of vector mesons is weaker in the present model than in the density-independent RMF models. This feature is common to all density-dependent RMF models [13,14,35]. They have a softer EOS than density-independent RMF models. However, the EOS of the present model is even softer than other density-dependent RMF models.

(ii) Our model contains also a point coupling interaction. Therefore short-range correction is included and the parameters of the mesons are not forced to reproduce energies and/or other physical quantities. Thus, the parameters of the OME potentials are almost fully determined by the long and intermediate range of the G-matrix potentials. As a result, the density dependence of the parameters is different in the present model and the density-dependent models without point coupling interactions. In the present model, the parameters of the vector mesons decrease more gradually than in other DDRMF models. Hence, the present model produces stronger repulsion. However, the σ meson parameters of the present model hardly change while those of DDRMF models decrease. Thus, the attraction of the present model produced by σ meson exchange is also stronger. Summing them up, the repulsion of the present model at high density is weaker than that of the DDRMF models without point coupling terms.

In this calculation, hyperons are not taken into account because there is a large uncertainty in hyperon interactions. Nevertheless we now discuss qualitatively the effect of the inclusion of hyperons. When hyperons appear in the EOS of neutron star matter, Σ^- is expected to be the first hyperon to appear in dense matter at a certain threshold density. The second hyperon expected to appear at higher threshold density is Λ_0. Hyperons appear due to the strangeness-changing weak processes. At the densities we are dealing with the inclusion of hyperons lowers the pressure of matter significantly compared with that of $npe\mu$ matter, because the neutrons with highest energy are replaced by low energy hyperons. As a result, EOS becomes considerably softer and the mass of the neutron star decreases by 0.3–0.6$\mathcal{M}_\odot$ by the inclusion of hyperons [54–56]. The deviation depends on the EOS of $npe\mu$ matter we adopt and on the hyperon-hyperon interaction introducing a large uncertainty in the effect of hyperons on $\mathcal{M}_{\max}$ due to the lack of the knowledge of this interaction.

The EOS of dense matter has to explain the measured neutron star masses. At least, those EOS's which predict $\mathcal{M}_{\max}$ lower than the neutron star mass measured most accurately must be excluded (because all compact objects with $\mathcal{M} > \mathcal{M}_{\max}$ are necessarily black holes). Namely, the heaviest measured neutron star mass $\mathcal{M}_{\rm obs}^{(\max)}$ implies the observational constraint:

$$\mathcal{M}_{\max}(EOS) > \mathcal{M}_{\rm obs}^{(\max)}, \tag{47}$$

where $\mathcal{M}_{\max}(EOS)$ is the maximum mass derived from the adopted EOS.

Thus, we focus our attention on the neutron stars with the heaviest measured masses. The present value is around $1.4\mathcal{M}_\odot \sim 1.5\mathcal{M}_\odot$. From the analysis of Vela X-1 [57], it has been found that Vela X-1 is at the 2σ confidence level $\mathcal{M}(2\sigma) > 1.54\mathcal{M}_\odot$. Comparing with this value, the present model is not excluded by measurements. There is a candidate which could push up the value of $\mathcal{M}_{\rm obs}^{(\max)}$ and exclude the present model. From the analysis of the mass of the neutron star in an X-ray binary, Cyg X-2, one finds at the 2σ confidence level $\mathcal{M}(2\sigma) = 1.78 \pm 0.46\mathcal{M}_\odot$ (i.e., $\mathcal{M}(2\sigma) > 1.32\mathcal{M}_\odot$), and the simultaneously determined mass of the companion star in Cyg X-2 is $\mathcal{M}_c = 0.60 \pm 0.13\mathcal{M}_\odot$ [58]. With an additional constraint on the companion mass, resulting from the theoretical models ($\mathcal{M}_X > 0.75\mathcal{M}_\odot$), Casares *et al.* obtain $\mathcal{M} > 1.88\mathcal{M}_\odot$ [59]. This would exclude the present model as far as the EOS is concerned. However, because of the additional assumptions and the strong model dependence, this cannot be used as a clean measurement of the neutron star mass. Therefore, the present model still survives. We can point out that the maximum mass $\mathcal{M}_{\max} = 1.59\ \mathcal{M}_\odot$ is very close to the measured values of neutron star masses, which are around 1.4 $\mathcal{M}_\odot$, while those derived from other RMF models are distributed above $\mathcal{M}_{\max} = 2.0\ \mathcal{M}_\odot$ [35].

VIII. SUMMARY

The goal of this paper was to investigate and to predict isospin properties of the nuclear many-body system on the basis of our knowledge of bare *NN*-interaction and the EOS of symmetric nuclear matter. We therefore constructed a RMF model with density dependent parameters consisting of one meson exchange terms and point coupling terms.

Starting from the bare *NN* interaction of Tamagaki and Takatsuka [22] which was determined so as to reproduce scattering data up to 350 MeV and by adopting the Brueckner formalism, we have derived a local approximation to the realistic effective G-matrix interaction in nuclear matter. It is represented in r-space. This interaction depends on the density of the medium. In the next step we introduced a covariant density functional, i.e., an effective relativistic Lagrangian with meson exchange terms in the four spin and isospin channels σ $(I = 0, T = 0)$, ω $(I = 1, T = 0)$, δ $(I = 0, T = 1)$, and ρ $(I = 1, T = 1)$ and the corresponding point coupling terms. The parameters of the meson exchange part were deduced by a fit of the corresponding nonrelativistic OME potentials to the radial shape of the G-matrix potentials at large and intermediate distances.

The density dependence of masses and couplings derived with the method discussed above is qualitatively consistent with some other relativistic models. The decreasing tendency of the meson masses m_ρ and m_ω and their mutual similarity are consistent with requirements of chiral symmetry and QCD oriented models [32–34]. They are also consistent with parameters adopted in other RMF models.

The short-range part of the effective interaction cannot be reproduced properly by effective meson exchange potentials. Therefore we introduced point-coupling terms in the four spin-isospin channels. They do not depend on the density and they contain only one adjustable parameter Λ. The form of these point coupling terms and in particular their isospin dependence

was taken from models based on chiral perturbation theory [4]. The parameter Λ has been adjusted together with the density dependent meson parameters to reproduce the EOS of symmetric nuclear matter.

In this way we derived a model based only on information on the properties of the free *NN* interaction and on the EOS of the symmetric nuclear matter without using any data concerning the isospin properties of the correlated system. It allows us to derive and predict not only properties of asymmetric nuclear matter close to the symmetric system as the asymmetry energy and its density dependence, but also the EOS for systems with arbitrary asymmetry parameter up to pure neutron matter. The predicted properties for asymmetry energy, such as the parameters $a_4 = 33.6$ MeV, $p_0 = 3.46$ MeV fm^{-3} and $\Delta K_0 = -106.9$ MeV are in a very good agreement with the empirical value of $a_4 = 33.2$ MeV [44] and with calculated results based on very successful phenomenological RMF parametrizations [14,15].

The results for pure neutron matter are in excellent agreement with non-relativistic many-body calculations of the Urbana group [23] up to rather high densities $\rho \simeq 3\rho_0$. Therefore we hope that the predicted isospin properties of our model are reliable. We therefore apply it also to the calculation of neutron stars and find agreement with empirical or observed data.

In particular we find that Fock terms play a crucial role for reproducing the saturation of isospin-symmetric nuclear matter. The EOS derived from the present model is softer than those of other RMF models, in particular at higher density. We have calculated the EOS in a neutron star and its configuration with maximal mass: $\mathcal{M}_{\max} = 1.59\mathcal{M}_{\odot}$, $R = 10.29$ km. This maximum mass is less than that derived from other RMF models, but appears rather consistent with measurements.

We would like to point out that the method we have proposed here allows us to determine isospin properties of the nuclear system with a realistic effective interaction, depending only on scattering data, while phenomenological RMF models use effective forces which are determined to a large extent by properties of nuclei in and close to the valley of stability. Therefore the present model can be expected to give us a wider range of applicability for the description of finite nuclei including very exotic nuclei.

ACKNOWLEDGMENTS

This work was carried out as a JSPS-DFG-joint project. It was supported in part by Grant-in-Aid for Specially Promoted Research (13002001) from the Ministry of Education, Science, Sport and Culture, by the JSPS Core-to-Core Program and by the 21st Century COE Program 'Quantum Extreme Systems and Their Symmetries (QUESTS).' One of the authors (P.R.) is grateful for its invitation program and the warm hospitality extended to him at the Department of Physics, University of Tokyo. One of the authors (M.S.) acknowledges financial aid from JSPS.

[1] J. D. Walecka, Ann. Phys. (NY) **83**, 491 (1974).
[2] B. D. Serot and J. D. Walecka, Adv. Nucl. Phys. **16**, 1 (1986).
[3] L. D. Miller and A. E. S. Green, Phys. Rev. C **5**, 241 (1972).
[4] N. Kaiser, S. Fritsch, and W. Weise, Nucl. Phys. **A697**, 255 (2002).
[5] D. Vretenar, T. Nikšić, and P. Ring, Phys. Rev. C **68**, 024310 (2003).
[6] J. Boguta and A. R. Bodmer, Nucl. Phys. **A292**, 413 (1977).
[7] P.-G. Reinhard, M. Rufa, J. Maruhn, W. Greiner, and J. Friedrich, Z. Phys. A **323**, 13 (1986).
[8] G. A. Lalazissis, J. König, and P. Ring, Phys. Rev. C **55**, 540 (1997).
[9] M. M. Sharma, M. A. Nagarajan, and P. Ring, Phys. Lett. **B312**, 377 (1993).
[10] Y. Sugahara and H. Toki, Nucl. Phys. **A579**, 557 (1994).
[11] Z. Y. Zhu, H. J. Mang, and P. Ring, Phys. Lett. **B254**, 325 (1991).
[12] R. Brockmann and H. Toki, Phys. Rev. Lett. **68**, 3408 (1992).
[13] S. Typel and H. H. Wolter, Nucl. Phys. **A656**, 331 (1999).
[14] T. Nikšić, D. Vretenar, P. Finelli, and P. Ring, Phys. Rev. C **66**, 024306 (2002).
[15] G. A. Lalazissis, T. Nikšić, D. Vretenar, and P. Ring, Phys. Rev. C **71**, 024312 (2005).
[16] C. Fuchs, H. Lenske, and H. H. Wolter, Phys. Rev. C **52**, 3043 (1995).
[17] F. de Jong and H. Lenske, Phys. Rev. C **57**, 3099 (1998).
[18] P.-G. Reinhard, Rep. Prog. Phys. **52**, 439 (1989).
[19] P. Ring, Prog. Part. Nucl. Phys. **37**, 193 (1996).
[20] D. Vretenar, A. V. Afanasjev, G. A. Lalazissis, and P. Ring, Phys. Rep. **409**, 101 (2005).
[21] M. Serra, T. Otsuka, Y. Akaishi, P. Ring, and S. Hirose, Prog. Theor. Phys. **113**, 1009 (2005).
[22] R. Tamagaki and T. Takatsuka, Prog. Theor. Phys. **105**, 1059 (2001).
[23] B. Friedman and V. R. Pandharipande, Nucl. Phys. **A361**, 502 (1981).
[24] K. A. Brueckner, Phys. Rev. **97**, 1353 (1955).
[25] S. Nagata, H. Bando, and Y. Akaishi, Prog. Theor. Phys. Suppl. **65**, 10 (1979).
[26] R. Machleidt, Adv. Nucl. Phys. **19**, 189 (1989).
[27] E. Schiller and H. Müther, Eur. Phys. J. A **11**, 15 (2001).
[28] S. O. Bäckmann, G. E. Brown, and J. A. Niskanen, Phys. Rep. **124**, 1 (1985).
[29] T. Matsuo, Ph.D. thesis, University of Tokyo (2004) (unpublished).
[30] T. Otsuka, T. Matsuo, and D. Abe, Phys. Rev. Lett. **97**, 162501 (2006).
[31] J. F. Berger, M. Girod, and D. Gogny, Comput. Phys. Commun. **61**, 365 (1991).
[32] T. Hatsuda and T. Kunihiro, Phys. Rev. Lett. **55**, 158 (1985).
[33] T. Hatsuda and T. Kunihiro, Prog. Theor. Phys. **74**, 768 (1985).
[34] T. Hatsuda and T. Kunihiro, Phys. Lett. **B185**, 304 (1987).
[35] S. F. Ban, J. Li, S. Q. Zhang, H. Y. Jia, J. P. Sang, and J. Meng, Phys. Rev. C **69**, 045805 (2004).
[36] T. Otsuka, R. Fujimoto, Y. Utsuno, B. A. Brown, M. Honma, and T. Mizusaki, Phys. Rev. Lett. **87**, 082502 (2001).
[37] T. Otsuka, Prog. Theor. Phys. Suppl. **146**, 6 (2002).
[38] T. Otsuka, Nucl. Phys. **734**, 365 (2004).
[39] T. Otsuka, Nucl. Phys. **722**, 347c (2003).

[40] M. Matsuo, Prog. Theor. Phys. Suppl. **146**, 110 (2002).
[41] H. Müther and A. Polls, Prog. Part. Nucl. Phys. **45**, 243 (2000).
[42] J. P. Blaizot, J. F. Berger, J. Dechargé, and M. Girod, Nucl. Phys. **A591**, 435 (1995).
[43] D. Vretenar, G. A. Lalazissis, R. Behnsch, W. Pöschl, and P. Ring, Nucl. Phys. **A621**, 853 (1997).
[44] P. A. Seeger and W. M. Howard, Nucl. Phys. **A238**, 491 (1975).
[45] R. J. Furnstahl, Nucl. Phys. **A706**, 85 (2002).
[46] V. E. Starodubsky and N. M. Hintz, Phys. Rev. C **49**, 2118 (1994).
[47] A. Krasznahorkay *et al*., Nucl. Phys. **A567**, 521 (1994).
[48] R. B. Wiringa, V. Fiks, and A. Fabrocini, Phys. Rev. C **38**, 1010 (1988).
[49] N. K. Glendenning, Nucl. Phys. **A493**, 521 (1989).
[50] G. Q. Li, R. Machleidt, and R. Brockmann, Phys. Rev. C **45**, 2782 (1992).
[51] T. Kasahara, Y. Akaishi, and H. Tanaka, Prog. Theor. Phys. Suppl. **56**, 96 (1974).
[52] J. R. Oppenheimer and G. M. Volkoff, Phys. Rev. **55**, 371 (1939).
[53] R. C. Tolman, Phys. Rev. **55**, 364 (1939).
[54] S. Nishizaki, T. Takatsuka, and Y. Yamamoto, Prog. Theor. Phys. **108**, 703 (2002).
[55] I. Vidana, A. Polls, A. Ramos, L. Engvik, and M. Hjorth-Jensen, Phys. Rev. C **62**, 035801 (2000).
[56] P. Haensel, "Final Stages of Stellar Evolution," edited by J.-M. Hameury and C. Motch, EAS Publications Series, EDP Sciences, 2003; arXiv:astro-ph/0301073.
[57] O. Braziv, L. Kaper, and M. H. Van Kerkwijk, Astron. Astrophys. **377**, 925 (2001).
[58] J. A. Orosz and E. Kuulkers, Monthly Notices of the Royal Astronomical Society **305**, 132 (1999).
[59] J. Casares, P. Charles, and E. Kuulkers, Astrophys. J. Lett. **493**, L39 (1998).